630

Chapter 1

Self-assembling Systems on Scales from Nanometers to Millimeters: Design and Discovery

LYLE ISAACS*, DONOVAN N. CHIN†, NED BOWDEN*, YOUNAN XIA*, AND GEORGE M. WHITESIDES*

**Harvard University, MA, USA*
†*Moldyn Inc., Cambridge, MA, USA*

1. INTRODUCTION

Self-assembly is the spontaneous organization of molecules or objects into stable aggregates by noncovalent forces [1–5]. Self-assembly is especially evident in biology and much of the early inspiration for studies of self-assembly came from biological aggregates: lipid bilayers, viral capsids, the DNA duplex, and the tertiary and quaternary structure of proteins [6–8]. Chemists have been exploring self-assembly as an alternative to the powerful, but stepwise, methods of synthetic chemistry [2,9–27]. Self-assembly is interesting both for its biological relevance, and because it is a new approach to complex structures having nanometer to millimeter dimensions that are difficult or impossible to prepare by traditional techniques. Figure 1 shows a scale from 1 nm to 10 mm; several examples of natural systems and their corresponding sizes are shown above the scale. Below the scale are pictures of four self-assembling systems that have been investigated in this group, namely hydrogen bonded self-assembled aggregates both in solution and the solid state, patterned self-assembled monolayers (SAMs) of alkanthiolates on gold, and milli-

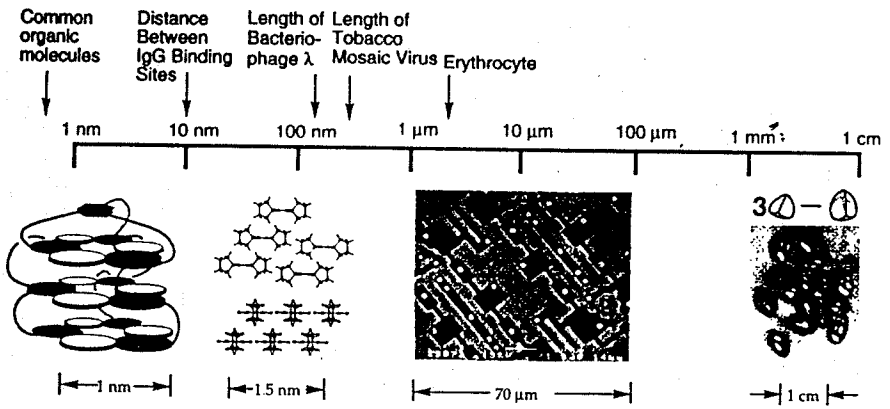

Figure 1 Illustration of the range of sizes of structures that can be formed by self-assembly. The sizes of several natural objects are included above the logarithmic scale for the purpose of comparison

meter-scale two- and three-dimensional self-assembled structures based on capillary forces: these systems form the basis of this review.

Many different types of forces have been explored for their ability to form self-assembled structures including: hydrogen bonds, metal–ligand interactions, hydrophobic interactions, electrostatic forces, and capillary forces. Receptor–ligand interactions and DNA duplex formation have also been used to form self-assembled structures. In this review we describe some of our experiences with self-assembly in four systems: aggregates in solution held together by networks of hydrogen bonds based on the cyanuric acid·melamine lattice [28,29], aggregates held together in the solid state by hydrogen bonds [30], SAMs of alkanethiols on gold [31,32], and mesoscale objects assembled using capillary forces [33–35]. Studies in self-assembly have often proceeded by designing the components, hypothesizing the outcome of the self-assembly process, preparing the components in the laboratory, and observing if a well-ordered assembly results experimentally. If an assembly forms, then it is characterized; if not, the program moves on to the next system. This hit-and-miss approach is inefficient. We have explicitly tried to develop systems that are stable, form reliably, and are amenable to systematic structural variation. The ability to make structural changes, and to observe the process resulting in self-assembly, has begun to allow us to understand the rules of self-assembly governing these systems and to make predictions about related structures.

2. SCOPE AND OBJECTIVES OF THE REVIEW

The scope of this review includes four areas of self-assembly that were investigated in this laboratory; namely self-assembly based on hydrogen bonds in solution, self-

assembly based on hydrogen bonds in organic molecular crystals, self-assembly of monolayers of alkanethiolates on gold, and self-assembly of macroscopic objects using capillary and other forces. The sections on aggregation in solution and the solid state will be limited to those systems where hydrogen bonds are a specific design element, characterization is extensive, and theoretical predictions of stability have been made. Self-assembly in natural systems and self-assembly in solution based on other forces are excluded from the review. The section on self-assembled monolayers will focus on the formation, structure, defects, and applications of SAMs and mixed SAMs of alkanethiols on gold. We do not include SAMs on substrates other than Au(111), or with ligands other than alkanethiols. The section on self-assembly of macroscopic objects will focus on assembly based on lateral capillary forces.

The objectives of this review are: to describe the types of structures that can be formed by self-assembly in these systems, to discuss the current experimental and theoretical issues of self-assembly, to assess the current role of theory in the predicting stability of self-assembled systems, and to highlight important future directions for self-assembled structures.

3. EXPERIMENTAL SYSTEMS

3.1 Soluble Hydrogen-bonded Molecular Aggregates

(a) Introduction

Organic chemistry has traditionally been concerned with the synthesis and characterization of *molecules* held together by *covalent* bonds. The great power and utility of organic synthesis is exemplified by the preparation of complex molecules such as vitamin B_{12}, palytoxin, and brevetoxin [36–39]. In recent years, however, increasing attention has been directed toward larger biomolecules; for example, peptides, proteins, oligosaccharides, RNA, and DNA. Much of the structure and function of these biomolecules is derived from noncovalent forces; namely hydrophobic and electrostatic interactions and hydrogen bonds. Often, these molecules are themselves aggregates of several molecules and are held together exclusively by intermolecular interactions. Based on this impetus, we and others have studied the ability of hydrogen bonds to direct the formation of aggregates [29]. Excellent reviews describing the work of other groups involved in this field are available [2,9,11,15,17,20,23]. The specific goal of this section is to describe the most important current issues in the design, synthesis, and characterization of aggregates based on the network of hydrogen bonds in the cyanuric acid·melamine lattice (CA·M). At the end of this section, the current limitations of and future challenges for self-assembly are discussed.

(b) Design

The focus of our research on hydrogen-bonded aggregates in solution is on one portion of the CA•M lattice, namely the cyclic hexameric "rosette", which is composed of three molecules of CA and M (Figure 2) [40]. We have concentrated on the hydrogen-bonded CA•M lattice for several reasons: hydrogen bonds are highly directional, the hydrogen-bonds are numerous (18 per rosette) and strong in chloroform solution (1–3 kcal mol^{-1} per hydrogen bond), and derivatives of CA and M are easily prepared by organic synthesis. The aggregation of several molecules to form a structured aggregate is an entropically disfavored process; the enthalpy of the interaction must overcome losses of translational, rotational, and conformational entropy.

We have used two strategies in the design of stable self-assembled aggregates based on the CA•M lattice; namely, preorganization [40] and peripheral crowding

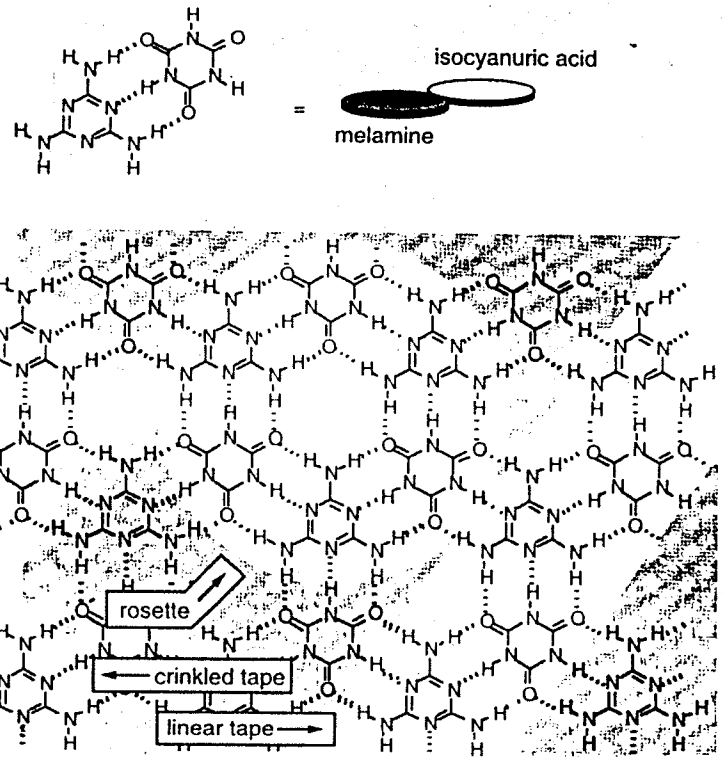

Figure 2 The structure of the hydrogen-bonded CA•M lattice. Three classes of aggregates that we have observed in solution and the solid state are highlighted: the rosette, crinkled tape, and linear tape motifs. The molecular structures of melamine and cyanuric acid and their abbreviated representation as dark and light disks are shown

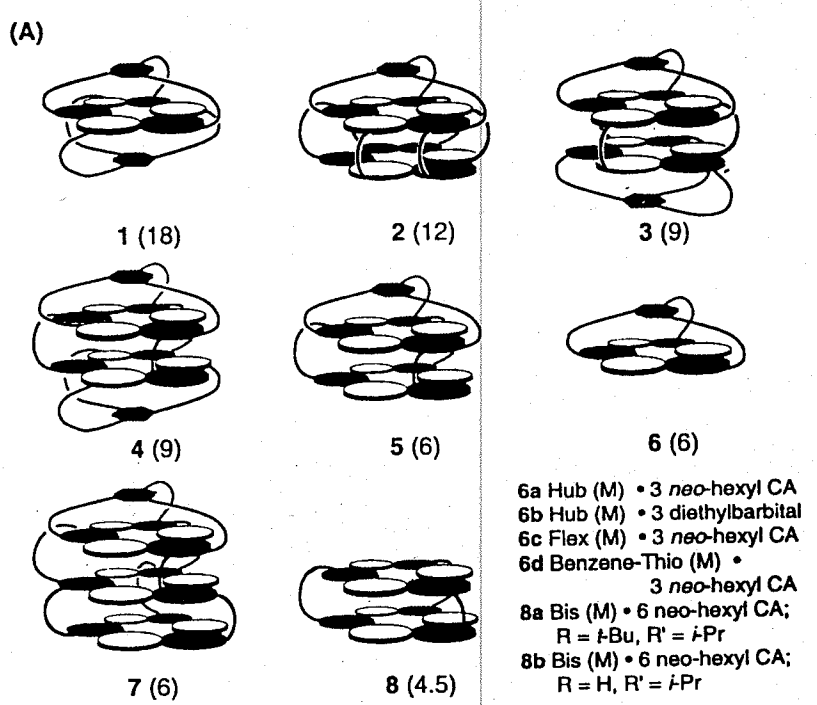

Figure 3 (A) Schematic representations of eight distinct classes of self-assembled structures (1–8). Aggregates 1–8 are arranged in decreasing order of stability; the number in parentheses is the ratio of the number of hydrogen bonds formed (HB) to the number of aggregating molecules minus one ($N - 1$) that we have used as a semiempirical parameter of stability.

[41]. Figure 3A shows eight distinct members (1–8) of this family of aggregates. The molecular structures of the components are shown in Figure 3B [40–48].

Preorganization Preorganization is a qualitative concept introduced by Cram [4] to describe the conformational similarity of a molecule in its uncomplexed relative to its complexed state. We have covalently linked the three melamines of the CA•M rosette by "spokes" to a central benzene-based "hub"; this linkage results in preorganization by reducing unfavorable changes in translational, rotational, and conformational entropy upon formation of the aggregate.

Peripheral crowding Peripheral crowding is a second strategy that produces stable aggregates based on the CA•M lattice [41]. Large substituents on CA and M develop severe steric interactions in certain configurations. These unfavorable steric interactions are less important in the cyclic rosette structure than in the linear or crinkled tape motifs (Figure 4) [41]. These steric interactions can be used to promote the formation of the rosette structure for these aggregates.

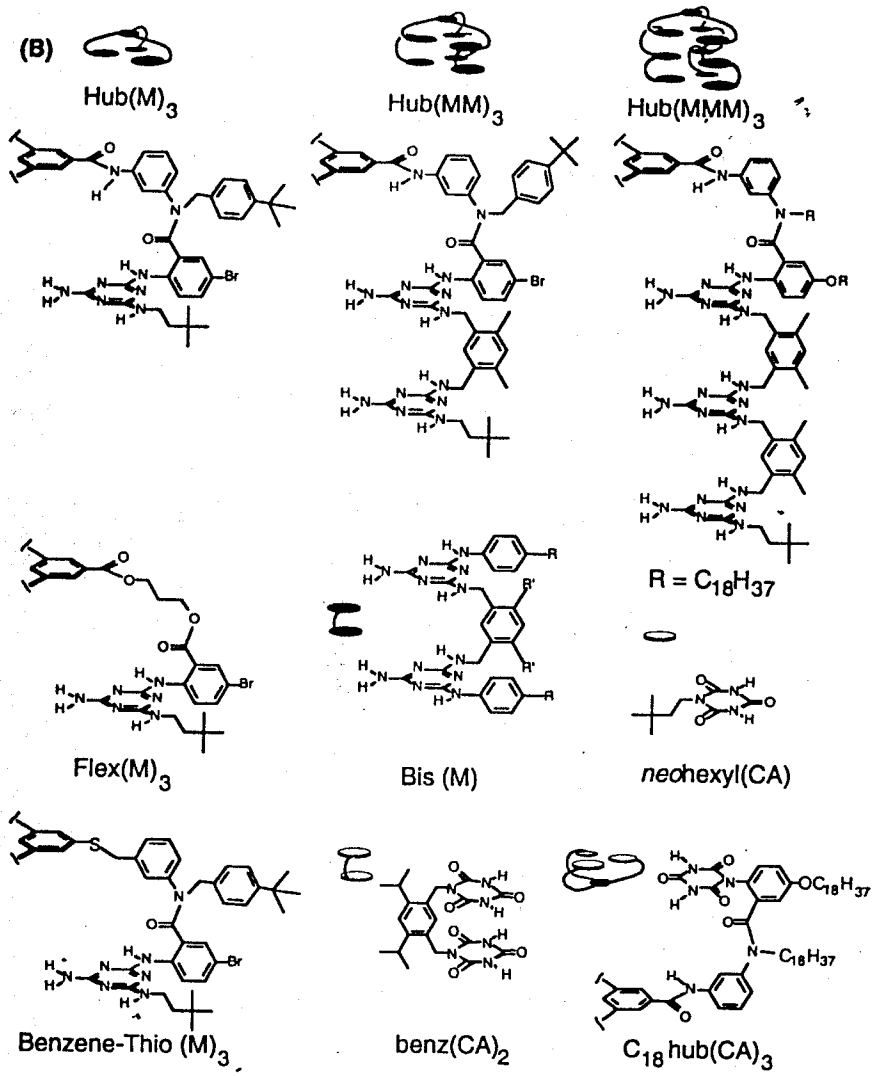

Figure 3 (B) Molecular and schematic representations of the components used in the formation of **1–8**

HB/N − 1 The stability of hydrogen-bonded aggregates based on the CA•M lattice is related to the number of hydrogen bonds (*HB*) formed upon aggregation and the total number of aggregating molecules (*N*) [28,49,50]. For the related series of aggregates shown in Figure 2, the quantity $HB/(N-1)$ is very useful predictor of relative stability. This ratio is intuitively reasonable; the enthalpy of aggregation is expected to increase as *HB* increases; the unfavorable losses of translational and

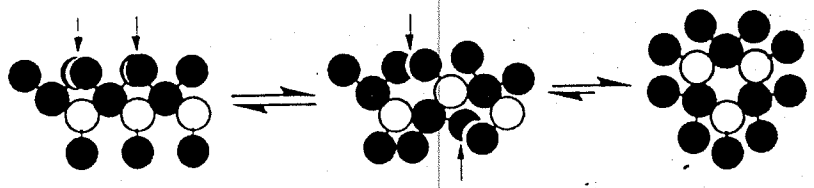

Figure 4 Incorporation of large groups (black disks) on the periphery of CA and M results in steric interaction between these groups in the tape (left) and crinkled tape (center) motifs, the arrows indicate these regions. In the rosette motif (right) these unfavorable steric interactions are minimized

rotational entropy upon aggregation is expected to increase as the number of particles in the assembly increases. In general, our experience suggests that $HB/(N-1)$ should be equal to or greater than six in order to achieve reasonably stable aggregates in the CA•M series in chloroform solution.

Symmetry In systems based on the CA•M lattice, the three points of connection of the spokes to the edge of the rosette can lead to C_3 or C_1 symmetry. Figure 5A shows a schematic representation of the two enantiomeric forms of C_3- and C_1-symmetric (**6**). It is useful to incorporate one or more potential elements of symmetry in the design of self-assembled aggregates. Products that possess these symmetry elements will show diagnostically simple NMR spectra, whereas structures that do not possess these symmetry elements will show more complex (and more difficult to analyze) spectra. Often, only a single structure for a self-assembled aggregate meets the symmetry considerations imposed by NMR spectral data and in these cases it is possible to use NMR spectroscopy to determine structure with few ambiguities [43,46,51]. Conversely, aggregates which are C_1 symmetric are particularly difficult to characterize; structure determination in these cases would require the powerful NMR techniques used for protein structure determination.

Solubility An important consideration in the design of self-assembled structures is solubility. The cyanuric acid and melamine components are often poorly soluble in chloroform; this insolubility hinders both synthesis and analysis of the self-assembled structure. We have often attached *t*-butyl benzyl, *t*-butyl phenyl, *n*-$C_{18}H_{37}$, and *neo*-hexyl groups to provide sufficient $CHCl_3$ solubility.

CPK models CPK models were used to help visualize the geometries of molecules and complexes in the design of aggregates **1–8**. These models are useful in identifying aggregates that *cannot* be stable due to impossible geometric constraints. They are *not* useful, in general, in determining the stability of a given aggregate, or even relative stability within a series of aggregates. Since CPK models are not calibrated for the weak intermolecular interactions that are so important in self-

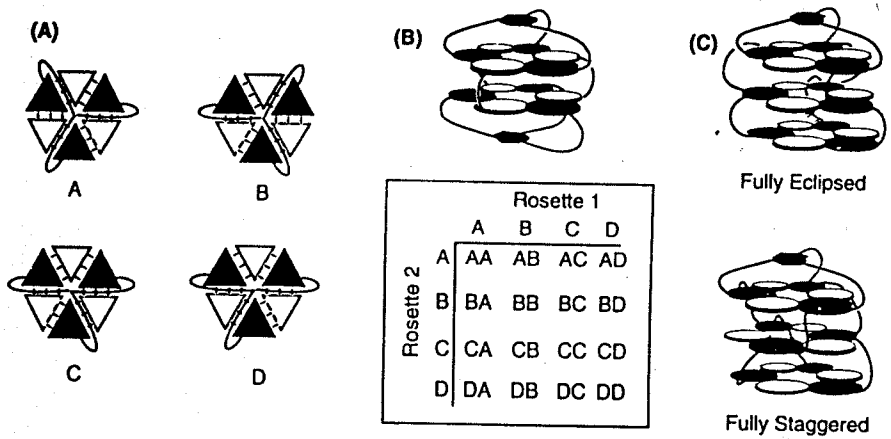

Figure 5 Aggregates 1–8 have the potential to exist as mixtures of isomers. (A) Schematic depiction of the four isomers possible for **6** resulting from different points of attachment of the spokes to the rosette. (B) Aggregate **3**, which contains two rosettes, can exist in 16 isomeric forms. This table enumerates the 16 possibilities based on the four isomers for a single rosette shown in (A). (C) Schematic depiction of the fully staggered and fully eclipsed isomers of **7**; only these isomers are compatible with the six lines in the imide region of the ^{1}H NMR spectrum

assembly, one must be cautious not to over-interpret the results inferred from examination of molecular models.

(c) Synthesis

The synthesis of noncovalent hydrogen-bonded aggregates can often be accomplished simply by mixing the components in the correct molar ratio in an appropriate solvent (usually chlorinated hydrocarbons such as chloroform). In some cases, one of the components (usually the cyanuric acids) may be poorly soluble in chloroform; in these cases it may be useful to dissolve the components in a more polar solvent or solvent mixture (e.g. chloroform–methanol), then remove this solvent and redissolve the residue in chloroform. This procedure can overcome kinetic limitations to formation of aggregates associated with solubilities.

(d) Characterization

Synthetic organic chemists have developed a powerful set of tools for the structural elucidation of synthetic or natural products. By applying these techniques it is often possible to provide *definitive proof* for the structure of a covalent molecule. Structural elucidation for aggregates is less direct and we have had to rely on

inference based on data obtained using several characterization methods. The most useful of these methods are nuclear magnetic resonance, gel permeation chromatography, vapor pressure osmometry (VPO), and electrospray mass spectrometry [28,51–53].

Nuclear magnetic resonance Several aspects of the NMR spectra of these hydrogen-bonded aggregates are noteworthy. These features are discussed here for the specific case of **6a** (Hub(M)$_3$·3 *neo*-hexyl (CA) (Figure 6A) [40].

Peak width The ^{1}H NMR spectrum of Hub(M)$_3$ in chloroform is broad and featureless except for solvent and *t*-butyl peaks (Figure 6A). This nondescript spectrum is the result of self-association and restricted rotation around the RNH–triazene bonds.

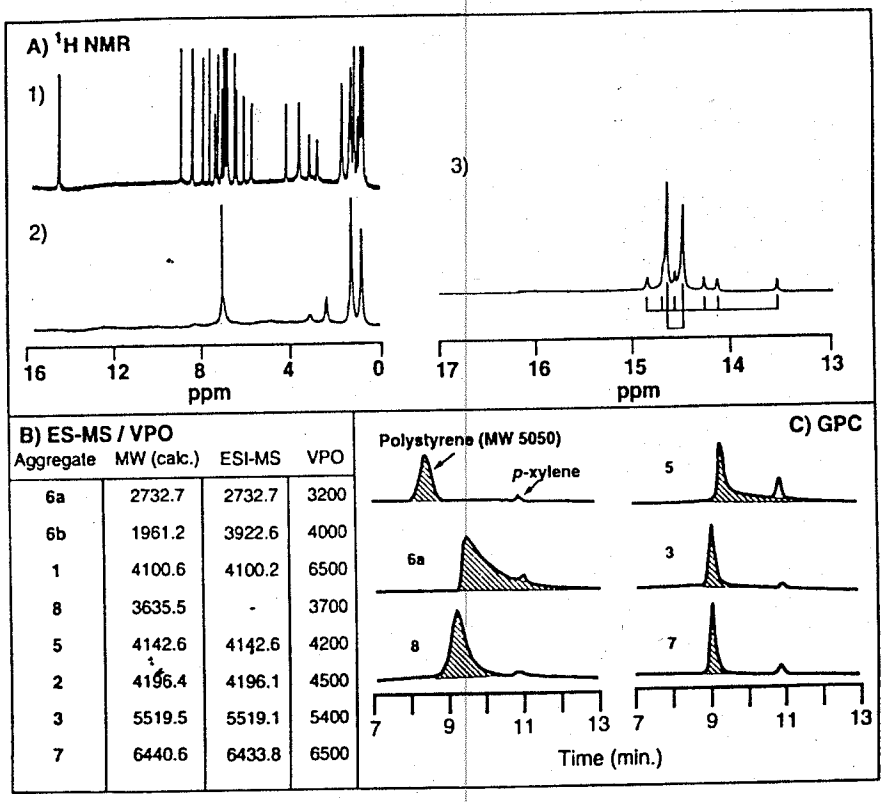

Figure 6 Characterization data for some noncovalent aggregates: (A) ^{1}H NMR spectra in $CDCl_3$ for 1) **6a**, 2) Hub(M)$_3$ and 3) and an expansion of the imide region for **6b**, (B) a table showing the calculated and experimentally determined (ES-MS and VPO) molecular weights for several aggregates; and (C) GPC chromatograms for five aggregates

Stoichiometry by titration The titration of $Hub(M)_3$ with solid portions of *neo*-hexyl CA can be monitored by ^1H NMR spectroscopy. Upon addition of three equivalents of *neo*-hexyl CA, the broad and featureless spectrum of $Hub(M)_3$ is transformed into the highly structured spectrum of **6a** (Figure 6A). At intermediate amounts of *neo*-hexyl CA, the spectrum is a combination of **6a** and free $Hub(M)_3$. Addition of *neo*-hexyl CA beyond three equivalents has no effect on the ^1H NMR spectrum; it is insoluble and visible as a white powder. These experiments are good evidence for the 1 : 3 stoichiometry.

Hydrogen bonded imide protons The hydrogen bonded N-H protons of the isocyanurate resonate in an uncluttered region of the ^1H NMR spectrum (13–16 ppm) [40,51,54]. The location and sharpness of these resonances is consistent with the presence of a highly structured hydrogen-bonded aggregate in solution. The number and intensity of these resonances is diagnostic for the time-averaged symmetry of the aggregate in solution [51]. In particular, only two resonances are observed in this region of the spectrum for **6a**. This observation implies that on the NMR time-scale, this aggregate has C_3 symmetry. The corresponding spectrum for **6b** ($Hub(M)_3$·3 diethylbarbital) shows eight resonances; two of higher intensity and six of lower, but equal intensity (Figure 6A). We rationalize this result by postulating two different aggregates, with C_3 and C_1 symmetries (Figure 5). In principle, these isomers can interconvert by rotation of the melamine about one of the aryl–NH triazene bonds.

^1H NMR: other aspects Two other aspects of the ^1H NMR spectrum of hydrogen bonded aggregates are useful in determining structure. Variable-temperature NMR can reveal dynamic processes that are fast (or slow) on the NMR time scale at room temperature [51]. Nuclear Overhauser effect (nOe) studies can be used to determine relative proximity of the hydrogen bonded protons and the diastereotopic methylene protons [40,43,46]. ^1H NMR competition studies where two different hubs (for example, $Hub(M)_3$ and $Flex(M)_3$) compete for only three equivalents of CA allows direct assessment of the relative stability of the competing aggregates [45,55].

Gel permeation chromatography GPC is a size-exclusion technique that provides information on molecular weight and stability of aggregates [41,43,44,46–48]. The pores of the stationary phase (cross-linked styrene/divinylbenzene) readily allow small molecules to enter, whereas larger molecules are excluded from these pores. The direct result is that smaller molecules take longer to pass through the column than larger molecules. Figure 6C shows the GPC traces obtained for **6a**, **8**, **5**, **3**, **7** and polystyrene ($MW = 5050$, polydispersity = 1.05) with added *p*-xylene as standard. The stability of these aggregates is reflected in the extent of their tailing on the column. Stable aggregates (e.g. **3** and **7**) elute from the column as sharp peaks. In contrast, kinetically more labile aggregates (e.g. **6a**, **8**, and **5**) dissociate on the GPC time scale (≈ 8 min) into their components; these components then

separate. These unstable aggregates appear as broadened, tailing peaks by GPC. The order of stability suggested by GPC correlates well with predictions based on the values of $HB/(N-1)$ and on ^1H NMR competition studies.

Vapor pressure osmometry VPO is a classical colligative property that yields a semiquantitative (number average) estimate of molecular weight in solution. Figure 6B shows the molecular weights determined by VPO for a series of aggregates. In general, the agreement between the calculated and experimentally determined molecular weight is within 20%. In the experiment, the voltage (and hence current) is recorded that is required to maintain a solution at known aggregate concentration at the same temperature as pure solvent while both undergo evaporative cooling. Comparing these voltages to those recorded for a series of standards of known molecular weight (in our case, sucrose octaacetate ($MW = 679$), polystyrene ($MW = 5050$), and perbenzoyl β-cyclodextrin ($MW = 3321$)) gives an estimate of the molecular weight of the unknown.

Electrospray ionization mass spectrometry ES-MS is a powerful tool for the analysis of bimolecular complexes and complexes containing metal cations. The success of these measurements relies on the ability of the complex to be ionized from suitable (usually aqueous) solvent systems. The aggregates described here are unstable in water, so a different ionization system was required. The use of the chloroform-soluble charge carrier tetraphenylphosphonium chloride, in experiments performed by Smith and coworkers, allowed the ionization of **6a** and its detection as **6a**·Cl^- [52,53]. Figure 6B shows the excellent agreement between the calculated and experimental values obtained for several other aggregates. Collision induced dissociation experiments of the m/z selected **6a**·Cl^- complex showed ions corresponding to $Hub(M)_3Cl^-$ and **6a**·Cl^-; this selectivity supports the suggestion that the self-assembly of **6a** in solution is a cooperative process.

(e) Discussion

Analysis of the spokes Many different mono-rosette aggregates, including (**6a–6d**, **6c**: $Flex(M)_3$·3 *neo*-hexyl CA, **6d**: benzene-thio$(M)_3$·3 *neo*-hexyl CA), have been prepared based on the "hub and spoke" architecture. On the basis of the number of hydrogen bonds formed and the number of particles aggregating, one might assume on the basis of the value of $HB/(N-1)$ that the stability of **6a–6d** would be similar. In fact, the stability of this series of aggregates depends on the nature of the "spokes" [42,49,50,56,57]. Compared to **6a** hubs incorporating thioether linkages (**6d**) or a propane diol linker (**6c**) form less stable aggregates (as determined by ^1H NMR spectroscopy, competition, and GPC studies). These results are readily rationalized; upon formation of the aggregates, larger losses in conformational entropy occur for **6c** and **6d** than for **6a** these losses result in a lower overall free

energy of binding. The entropic cost of freezing a n-fold free rotor in a single conformation can be approximated by Equation 1 [50,57].

$$T\Delta S = -RT \ln n \quad (1)$$

Thus, the rigid amide bonds and benzene rings in $HubM_3$ are less costly to restrict conformationally than are the three-fold rotors in $Flex(M)_3$ and benzene-thio$(M)_3$.

Peripheral crowding and buttressing groups Peripheral crowding refers to the steric interaction between substituents on the periphery of an aggregate; these steric interactions can be used to favor the formation of the rosette over tape and crinkled tape motifs (Figure 4) [41]. For example, aggregate **8a** (Bis(M)·3 *neo*-hexyl CA, R = *t*-Bu, R′ = *i*-Pr) is formed and is stable in chloroform solution, while aggregate **8b** (Bis(M)·3 *neo*-hexyl CA, R = H, R′ = *i*-Pr), which incorporates the less bulky phenyl group, does not form a well defined aggregate on mixing the components in chloroform. Another important factor governing the stability of **8a** (and also **2**–**5** and **7**) is the incorporation of the isopropyl (or methyl) groups on the phenylenediamine linker [41]. These isopropyl groups act as buttressing groups and preorganize the melamines (or CA in the case of **2** and **3**) to lie in parallel orientation. When these isopropyl groups are removed (Bis(M)·3 *neo*-hexyl CA, R = *t*-Bu, R′ = H) no stable aggregate formed.

Isomers As described above, aggregate **6** can exist in two isomeric forms, namely C_3- and C_1-**6** (Figure 5). An important goal of this research program is the synthesis of large, structurally complex aggregates. Toward this goal, we investigated the design, synthesis, and characterization of aggregates incorporating two or more rosettes stacked in parallel orientation, (**3**–**5** and **7**) [41–43,46,47]. The potential isomerism in these aggregates is more complex than in aggregates based on a single rosette. For **3**, sixteen isomeric aggregates differing only in the relative orientation of the spokes are possible (Figure 5B). The ^{1}H NMR spectrum of **3** showed only two resonances in the imide region. Symmetry considerations, therefore, rule out all but three of the possible isomers; namely, the enantiomeric pairs D_3-AA and D_3-BB and the meso compound C_{3h}-AB. It was not possible to distinguish between these possibilities on the basis of NMR spectroscopy, but computational results suggest that C_{3h}-AB is less stable than D_3-AA and D_3-BB due to unfavorable eclipsing interactions between the phenyl groups [54].

The most complicated aggregate that has been prepared to date is **7** [46]. Aggregate **7** consists of a nona-melamine derivative, $Hub(MMM)_3$, and nine molecules of *neo*-hexyl CA comprising three connected parallel rosettes. Aggregate **7** is held together by 54 hydrogen bonds and has a weight of 6.4 kD – slightly larger than a small protein like insulin. As for **3**, many (16) isomers are possible, but ^{1}H NMR of the aggregate shows only six resonances in the imide region. These six resonances result from three independent C_3-symmetric rosettes contributing two resonances each. Only the fully eclipsed and fully staggered conformations shown in

Figure 5C are consistent with these symmetry constraints. We have not been able to distinguish between these isomeric forms. These observations serve as a warning: it may be possible to synthesize relatively complex aggregates like **7**, but in the absence of symmetry their characterization will remain challenging.

(f) Attempted synthesis of tetrahedral aggregates

We have investigated the possibility of forming aggregates in which a CA·M rosette is held on each face of a tetrahedron [55,58]. Such tetrahedral aggregates would be a step toward structurally complex and potentially functional aggregates (the central cavity could, for example, act as a receptor for guest molecules). Figure 7 shows the molecular structure of the two components and a schematic drawing of the proposed tetrahedral aggregate. Each tetrahedron would be composed of ten individual particles; four equivalents of tris-M would be situated at the corners of the tetrahedron, and six equivalents of bis-CA bridge each edge of the tetrahedron. The proposed aggregate would be held together by 72 hydrogen bonds; yielding a value of $HB/(N-1) = 8$. A homogeneous solution of the components in hot chloroform–methanol could be formed, but upon cooling and concentration only $CHCl_3$-insoluble gels were formed. These results were discouraging since we predicted stability for this aggregate *a priori* based on examination of CPK models and $HB/(N-1)$. We believe that instability in this case is due to two factors: insufficient preorganization, and an unfavorable $\Delta\Delta G$ of solvation; there is a high entropic price to trap solvent molecules inside the tetrahedral cavity.

(g) Future challenges and unsolved problems

Despite our success in predicting and understanding the series of aggregates based on connected stacks of CA·M rosettes, we have not yet been able to extend this

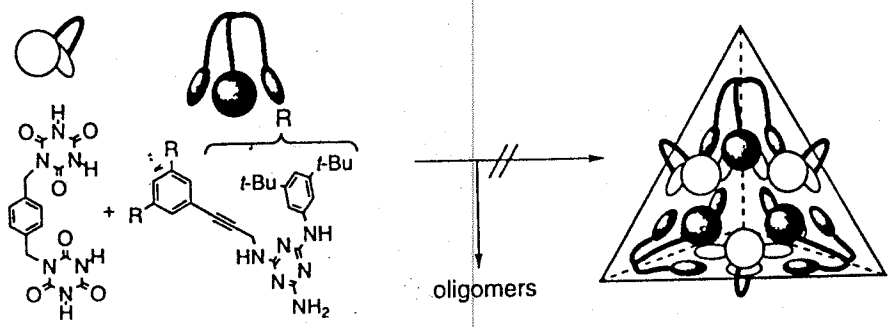

Figure 7 Molecular structures and schematic representations of a bis-CA and a tris-M that *do not* self-assemble to form the proposed tetrahedral aggregate: oligomers are formed preferentially

platform beyond parallel stacked rosettes [58]. We also have not yet been able to make very large aggregates. Our unsuccessful efforts directed toward the synthesis of tetrahedral aggregates underscore this point; despite our best efforts at design we were unable to synthesize stable aggregates. Clearly, there are terms that contribute to the ΔG of aggregation as well as intra- and intermolecular forces that we do not yet understand well. One particular deficiency is that CPK models are *not* helpful in predicting the stability of structures involving noncovalent forces. Improved methods (computational or otherwise) for the construction, manipulation, and evaluation of potential self-assembled structures as well as improved methods for the characterization of nonsymmetrical aggregates would be useful and important advances.

An important future concern for self-assembly is the construction of aggregates with function. None of the aggregates that we have synthesized to date are functional. Some steps have been taken in this direction by Rebek who has made dimeric aggregates that show molecular recognition properties and by Ghadiri who has made artificial membrane channels [9,12]. Without some demonstrated utility, this type of self-assembly remains an interesting, but academic, exercise in design. An equally important concern for future work in self-assembly is the solvent. Most of the self-assembled hydrogen bonded structures prepared have been designed to assemble in chlorinated hydrocarbons. In contrast, the interesting examples of biological self-assembly take place in water. A clear current limitation of molecular self-assembly is our inability to take advantage of the hydrophobic effect to construct aggregates that are both structured, soluble, and stable in water.

3.2 Molecules on Surfaces: Self-Assembled Monolayers

Self-assembled monolayers (SAMs) are highly ordered molecular assemblies that form spontaneously by chemisorption and self-organization of functionalized long-chain molecules on the surfaces of appropriate substrates [59]. They represent the best developed class of nonbiological systems involving self-assembly. They are robust, relatively stable, and capable of providing the flexibility, both at the individual molecular and materials levels, required to tailor the properties of surfaces [32,60]. Various types of systems of SAMs have been developed (Table 1), and a number of reviews have been devoted to this subject [32,59,61–63]. This section will focus on SAMs of alkanethiolates on thin polycrystalline films of gold since they are the most studied, and certainly the best characterized, system to date [64]. We shall outline the formation, structure, order, and defects of SAMs and their applications in interface engineering and microfabrication.

The process of spontaneous formation of *ordered* structures that occur as reaction, adsorption, and organization of alkanethiols ($X\text{-}(CH_2)_n\text{-}SH$) on gold is a good example of molecular self-assembly [1,31]. Their construction is driven by the thermodynamically favored segregation of molecules to the phase boundary between solid gold and solution (or vapor) of alkanethiols. The chemical bonding between

Table 1 Substrates and ligands that form self-assembled monolayers (SAMs)

Substrate	Ligand or precursor	Binding	Ref.
Au	RSH, ArSH (thiols)	RS–Au	62
Au	RSSR′ (disulfides)	RS–Au	87
Au	RSR′ (sulfides)	RS–Au	150
Au	RSO_2H	RSO_2–Au	151
Au	R_3P	R_3P–Au	152
Ag	RSH, ArSH	RS–Ag	153
Cu	RSH, ArSH	RS–Cu	154
Pd	RSH, ArSH	RS–Pd	155
Pt	RNC	RNC–Pt	156
GaAs	RSH	RS–GaAs	157
InP	RSH	RS–InP	158
SiO_2, glass	$RSiCl_3$, $RSi(OR')_3$	siloxane	159
Si/Si–H	$(RCOO)_2$ (neat)	R–Si	160
Si/Si–H	$RCH{=}CH_2$	RCH_2CH_2Si	161
Si/Si–Cl	RLi, R–MgX	R–Si	162
metal oxides	RCOOH	$RCOO^- \cdots MO_n$	163
metal oxides	RCONHOH	$RCONHOH \cdots MO_n$	164
ZrO_2	RPO_3H_2	$RPO_3^{2-} \cdots Zr(IV)$	165
In_2O_3/SnO_2 (ITO)	RPO_3H_2	$RPO_3^{2-} \cdots M(n+)$	166

sulfur atoms and gold on the surface ($\approx 44\,kcal\,mol^{-1}$) drives the assembly; sulfur atoms anchored on the surface bring the alkyl chains of these molecule into close contact, freezing out configurational entropy, and leading the chains to order [62]. The degree of interaction in a SAM increases with the density of molecules on the surface and the length of the alkyl backbones. As a result, only alkanethiolates with $n > 11$ form closely-packed, highly-ordered, and effectively two-dimensional organic quasicrystals on the surfaces of gold [62]. The nomenclature of materials science is not fully in accord with organic chemistry in the use of the term of "self-assembly": systems in which only chemisorption was involved, and neither monolayers nor ordered structures were formed, have also been called SAMs.

(a) Fundamental studies on SAMs

SAMs of alkanethiolates on gold have been characterized using a wide range of techniques (Table 2). Because optical and diffraction techniques can only reveal the properties of SAMs averaged over probed areas that are typically a few square millimeters in size, scanning probe microscopy (SPM) is increasingly used to study SAMs, and in particular, to characterize their structure and order [62,65]. Application of SPM to SAMs has, however, been more complicated than anticipated. There is still no good model to account for what occurs when a metallic tip approaches a gold surface that has been covered with a 1–2 nm thick layer of insulating SAMs

Table 2 Methods for the characterization of SAMs by alkanethiolates on Au

Property of SAMs	Technique	Refs.
Structure and order	Scanning probe microscopy (STM, AFM, and LFM)	62, 65
	Infrared spectroscopy	61, 167
	Low energy helium diffraction	168
	X-ray diffraction	169
	Transmission electron diffraction	170
	Surface Raman scattering	171
	Sum frequency spectroscopy (SFS)	172, 173
Composition	X-ray photoelectron spectroscopy (XPS)	174
	Temperature programmed desorption (TPD)	175
	Mass spectroscopy (MS)	69, 176
Wettability	Contact angle	177
Thickness	Ellipsometry	178
Coverage and/or degree of perfection	Quartz crystal microbalance (QCM)	71
	Surface acoustic wave device (SAWD)	179
	Electrochemical methods	180, 181
Defects	STM and AFM	62
	Wet etching	78

[62]. Explaining the SPM image requires caution. For example, the hexagonal lattice observed in early scanning tunneling microscopy (STM) studies [66] that used high currents (≈ 1 nA) is now believed to be the image of the sulfur atoms rather than the head groups of a SAM [62]. The structure of the outer surface of a SAM (for example, the superlattice) can only be observed using STM operated at ultralow currents (<10 pA). The contrast in the STM image acquired at a constant current provides a positive record of the topology of the SAM. The SPM technique is now showing a rich variety of surface structures (or phases), and more importantly, it is providing a flood of useful information about the origin and distribution of defects in SAMs [62,65].

Formation of SAMs SAMs of alkanethiolates on gold can be easily prepared by spontaneous adsorption of alkanethiols onto gold, either from solution or vapor phase. Although it is generally accepted that the reaction involved can be expressed as (2),

$$\text{X–R–SH} + \text{Au(0)}_n \longrightarrow \text{X–R–S}^-\text{Au(I)}\cdot\text{Au(0)}_{n-1} + \tfrac{1}{2}\text{H}_2 \qquad (2)$$

the mechanistic details of the reaction of alkanethiols with the gold surface are still not completely understood. For example, the fate of the hydrogen atom, and the exact nature of the resulting species on the gold surface is not well-established. A recent X-ray diffraction study suggested that the species on the Au surface is a disulfide (X–R–S–S–R–X) rather than a thiolate (X–R–S$^-$), although this suggestion

requires physically unreasonable bond lengths and results from a sample in which the potential radiation damage was high [67]. Recent studies based on mass spectrometry also indicated that SAMs prepared from solutions of alkanethiols in the ambient atmosphere of a laboratory are a mixture of X–RS$^-$, X–RSO$_2^-$, and X–RSO$_3^-$ since air oxidation of alkanethiolate solutions occurs very rapidly [68,69].

The kinetics of the formation of SAMs on gold has been studied using a number of techniques; ellipsometry [70], contact angle [70], quartz crystal microbalance [71,72], and surface acoustic wave [71]. These studies found that the growth rate was proportional to the number of unoccupied sites on gold, and could be described as a first-order Langmuir adsorption process. Most of these techniques were, however, spatially averaging, and thus left questions about the microscopic aspects of self-assembly unanswered. Poirier and Pylant studied the microscopic mechanism for the formation of closely-packed structures of alkanethiolates on the surfaces of gold using ultrahigh vacuum (UHV) STM [73]. They suggested a molecular-scale picture for the self-assembling process in which the alkanethiols form the following phases with increasing coverage: a lattice-gas phase, a low-density solid phase, and a higher density solid phase (Figure 8). This growth model has been observed in several systems, including SAMs of $HSC_6H_{12}COOH$ and $HSC_9H_{18}CH_3$ from the vapor phase, and SAM of $HSC_9H_{18}CH_3$ from the solution; this mechanism appears to be a general one for the self-assembly of alkanethiolates on gold [73].

Structure and order of SAMs It is generally accepted that sulfur atoms form a $\sqrt{3} \times \sqrt{3}$ R30° overlayer structure on the Au(111) surface [62]. To maximize the van der Waals interactions between adjacent methylene groups (≈ 1.5 kcal mol^{-1} per CH_2) the chains tilt at an angle of $\approx 30°$ from the surface normal [61]. The alkyl chains, however, may have several different conformations, and thus form a "superlattice" at the surface of the monolayer [74,75]. These results indicate that the order in the top part of SAMs is not dictated by the sulfur atoms directly bonded to the gold, but also strongly depends on the intermolecular interaction between the alkyl chains. When alkanethiolates are terminated with head groups other than the methyl group, it becomes even more complicated to predict and determine the structures of the formed SAMs [62]. In fact, it has been shown that the end group (in particular, a bulky end group) may play the most important role in determining the packing and order of a SAM [76].

Defects in SAMs The density of defects in SAMs may ultimately determine the usefulness of the materials in micro- and nanofabrication [77]. Although SAMs are representative self-assembling systems and tend to reject defects, formation of defects in these systems is inevitable because the true thermodynamic equilibrium is never achieved in the preparation of a SAM. A variety of factors have been found to influence the formation and distribution of defects in a SAM, including the molecular structure of the surface, the length of the alkyl chain, and the conditions used to prepare the SAM [78]. A range of techniques have been employed to

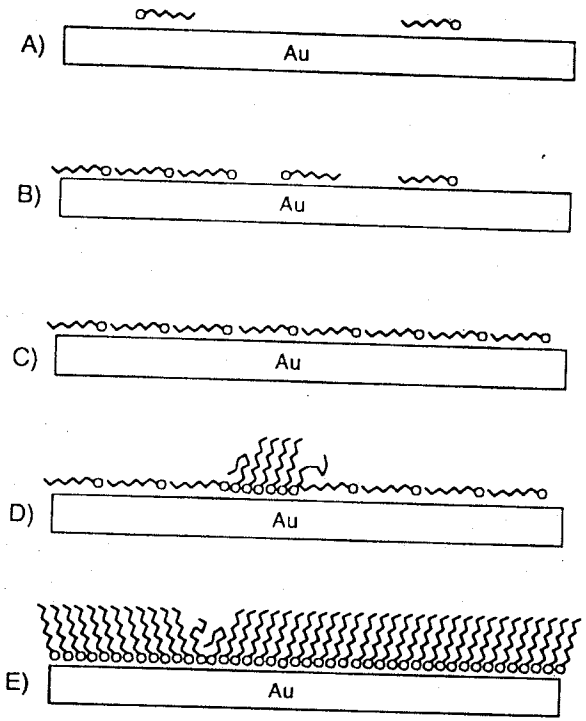

Figure 8 Schematic illustration for the formation of SAMs of alkanethiolates on gold [73]. (A) Alkanethiols adopt the highly mobile lattice-gas phase; (B) above a critical value of coverage, striped-phase islands are formed; (C) surface reaches saturation coverage of striped phase; (D) surface undergoes lateral-pressure-induced solid phase transition: high-density islands nucleate and grow at domain boundaries; (E) high-density islands grow at the expense of the striped phase until the surface reaches saturation

evaluate and characterize the defects in SAMs (Table 2). These techniques are complementary to each other; the electrochemical method only provides a statistical picture of defects over a relatively large area; SPM methods can only collect information over a relatively small area, but can provide useful information about the nature and origin of defects. A combination of these techniques, therefore, seems to be the most appropriate way for the characterization of defects in SAMs.

Figure 9 shows a high resolution STM image of the SAM of dodecanethiolate on the surface of Au(111) [62]. The black lines are now believed to be depressions in the monolayer where neighboring thiols have either tilted over or migrated to cover missing lines of thiols. The inset shows the STM image of a similar sample at a molecular resolution. The gold terrace shown here had five depressions (black "holes") that are one gold step (≈ 0.24 nm) in depth. These depressions are pits in gold rather than defects in SAMs; they are still covered with an ordered SAM with a lattice characteristic of the packing of molecules in the SAM on the flat surface. The origin of these pits is still under debate; they could originate from a corrosion

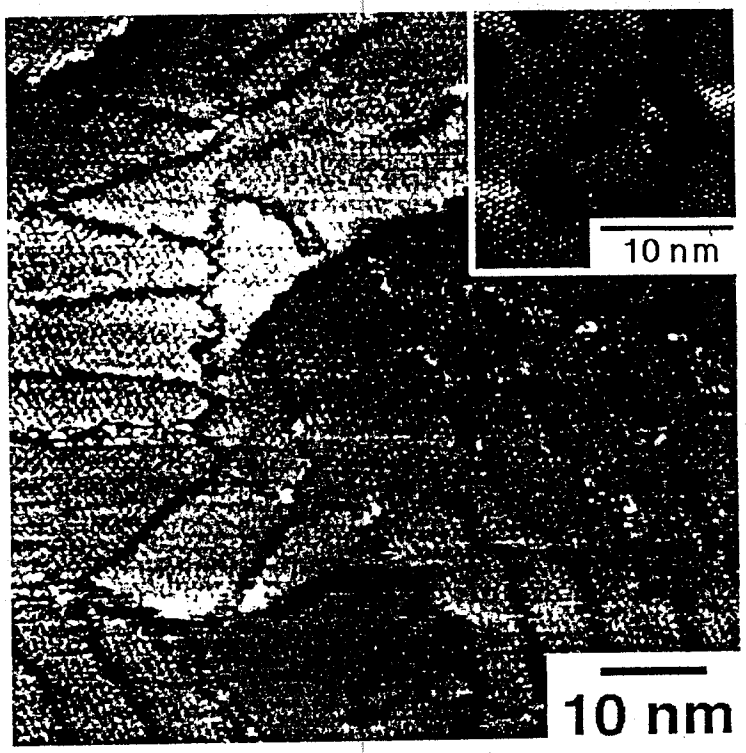

Figure 9 Scanning tunneling microscopy (STM) image of a SAM of dodecanethiolate on Au(111) that shows a gold step, a screw dislocation, and depressed lines in the monolayer due to the accommodation of missing lines of thiols by vicinal molecules. The inset shows five pits in gold that were ≈ 0.24 nm deep and linked by domain boundaries. The monolayer packing corresponds to a phase of the c(4*2) rectangular superlattice. These images were provided by Biebuyck and coworkers [62]

process or from a reconstruction of the gold surface caused by the adsorption of the thiols [79,80].

Current estimates for the number of pinholes in SAMs of hexadecathiolate on Au range from two to several thousand per square centimeter, with the latter value being more realistic. Thermal annealing induces reorganization of the SAM and the surface, and usually reduces the density of pits in SAMs by migration and coalescence of pits in gold with steps [81]. A recent study using a wet-chemical etchant to amplify the defects in SAMs gave $\approx 90\,\text{pits}\,\text{mm}^{-2}$ as a minimum value for the density of defects for a SAM of hexadecanethiolate on 20 nm thick gold [78]. Preparation of truly defect-free SAMs still remains a great challenge in this area.

Mixed SAMs The preparation of SAMs with more than one head groups and/or chain lengths is a prerequisite for many of their uses in the design and synthesis of interfaces with complex properties [32,60,82,83]. With the development of SPM

techniques, more and more information has become available on the structure and order in mixed SAMs [84,85]. In contrast to what is known about mixed Langmuir–Blodgett (LB) films [86], no phase segregation occurs at scales larger than 50 nm for two-component SAMs on gold surface. Asymmetric disulfides (RS–SR′) provide a good system for the study of phase segregation in mixed SAMs because the adsorption of disulfide on gold leads to two equal populations of end groups in the formed SAM [84,85,87]. STM images showed that the two components (for example, $-CH_3$ and $-OH$) in the SAM are well mixed without disruption of the packing in the monolayer [88].

(b) Applications of SAMs in interface engineering and microfabrication

SAMs of alkanethiolates on gold exhibit many of the features that are most attractive about self-assembling systems: ease of preparation, relatively low density of defects, good stability under ambient laboratory conditions, and amenability to the control over the interfacial (for example, physical, chemical, electrochemical, and biochemical) properties [32,59]. SAMs have been used as active elements to fabricate sensors and biosensors [89,90]; they may also be useful in fabricating capacitors and molecular electronic devices [91]. Equally importantly, SAMs are capable of protecting the underlying surfaces from certain chemical etchants, a characteristic that may have a number of potential technological applications. Early studies showed that SAMs of alkanethiolates on Cu and GaAs can inhibit oxidation by retarding oxygen transport to the surface [92,93]. We, and others, recently demonstrated that SAMs can be directly used as nanometer-thick resists in chemical etching; this capability combined with appropriate printing techniques is the basis for methods of fabricating micro- and nanostructures [77,94,95]. Fabrication procedures involving SAMs are relatively low-cost compared with conventional photolithographic methods.

Patterning SAMs in the plane of the monolayer has been achieved using a wide range of techniques (Table 3). Among these techniques, microcontact printing (μCP) is the one that seems to offer the most interesting combination of convenience and new capability (Figure 10). Microcontact printing forms patterned SAMs by contact of an elastomeric stamp (usually made from polydimethylsiloxane, PDMS) wetted with (or containing dissolved) alkanethiols, with a gold or silver surface [77]. It provides a superior control over the surface chemistry. Printing has the advantage of simplicity and convenience: multiple copies of the pattern can be easily reproduced using a straightforward procedure. It is a inherent parallel process; areas as large as $\approx 50\,cm^2$ can be patterned with submicron features on a single impression [96]. A recent, thoughtful study by Larsen *et al.* showed that μCP formed SAMs of dodecanethiolate on Au(111) that were indistinguishable from those formed from solutions of dodecanethiol, when the ink concentration was >10 mM and the duration of contact was >0.5 s [74].

Table 3 Methods that have been used for patterning SAMs of thiolates

Technique	SAMs	Resolution[a]	Refs.
Microcontact printing (μCP)			
	RSH/Au	≈35 nm	97
	RSH/Ag	≈100 nm	102
	RSH/Cu	≈500 nm	182
Photo-oxidation	RSH/Au	≈10 mm	183, 184
Photo-cross-linking	RSH/Au	≈10 mm	185, 186
Photoactivation	RSH/Au	≈10 mm	187, 188
Electron beam writing	RSH/Au	≈75 nm	189
	RSH/GaAs	≈25 nm	190
Focused ion beam writing	RSH/Ag	≈10 mm	191
Neutral metastable atom writing	RSH/Au	≈70 nm	192
SPM lithography	RSH/Au	≈10 nm	193
Micromachining	RSH/Au	≈100 nm	194
Micropen writing	RSH/Au	≈10 mm	195

[a] The lateral dimension of the smallest feature that has been generated.

Microcontact printing has been used to form patterned SAMs of alkanethiolates on Au, Ag, Cu and GaAs; and of alkylsiloxanes on Si/SiO_2 and glass [95]. Patterned features as small as ≈500 nm in dimensions can be routinely generated using μCP; smaller features (≈35 nm) have also been fabricated with greater difficulty and lower reproducibility [97]. The lower limit for the resolution in this technique, the upper limit of the area that can be patterned on one contact, and the degree to which multiple impressions can be brought into registration, have yet to be established.

The ability to form patterned SAMs allows us to engineer the interfacial properties of a surface with one more degree of freedom, in addition to the flexibility offered by SAMs themselves. It provides immediate opportunities to prepare systems in which structures can be controlled *in* the plane of the interface. SAMs can be used to control the nucleation, adsorption, and wetting of other materials, and thus patterned SAMs can be used as templates to direct and control the assemblies of other materials to form useful structures; they can also be used as patterned resists in directing the dissolution of the substrate to form patterns and structures in the underlying substrates (Au, SiO_2 and Si) [95].

Figure 11A shows an optical micrograph of water drops preferentially condensed on hydrophilic SAMs terminated by carboxylic (COOH) groups; no water condensed on the hydrophobic SAMs terminated by methyl (CH_3) groups [98]. This process shows how the functionality of a SAM influences the condensation of water vapor on a SAM-derivatized surface. It uses self-assembly at two scales: the formation of SAMs at the molecular scale and the directed condensation of water vapor at the macroscopic scale. The organization of liquids into patterned arrays illustrates one of the uses of self-assembly in microfabrication [99].

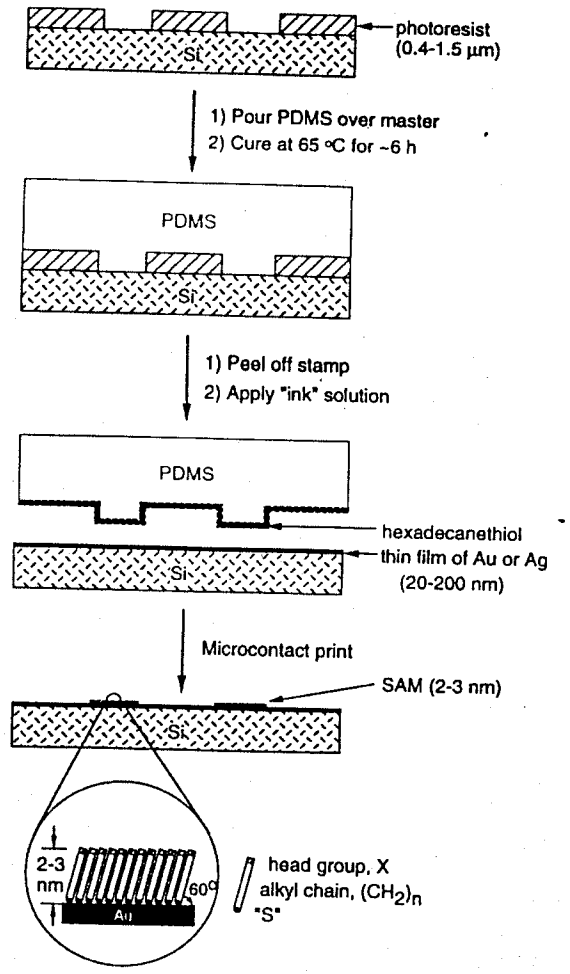

Figure 10 Schematic illustration of the procedure used for microcontact printing of hexadecanethiol on gold

Patterned SAMs can also be used as templates to define and control the adsorption of extracellular matrix proteins, and consequently the attachment of mammalian cells [100,101]. Figure 11B shows an SEM image of cells that have been selectively attached to a surface patterned with SAM. Using a very simple procedure for patterning, it is possible to dictate the shape of a cell that is attached to a surface, and thus partially control cell growth and protein secretion. This technique allows us to examine the influence of cell morphology on cell metabolism, and should be useful for applications in biotechnology that require analysis of individual cells cultured at high density, or for repeated access to cells placed in specified locations.

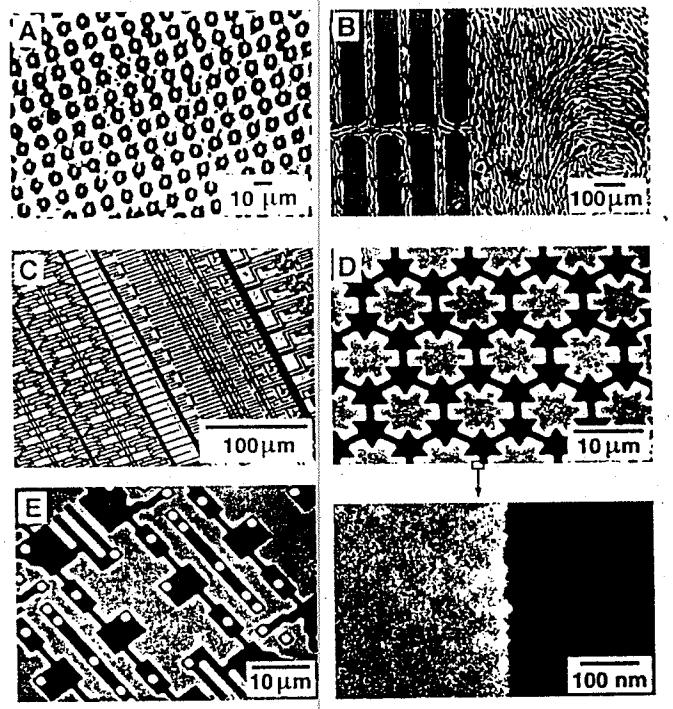

Figure 11 (A) An optical micrograph of water selectively condensed on a SAM-patterned surface of gold [98]; (B) an SEM image of cells selectively attached to a surface using patterned SAMs as templates [100,101]; (C–E) SEM images of test patterns of silver fabricated by μCP with hexadecanethiol, followed by selective etching in an aqueous ferricyanide solution [102]

Figures 11C–E show SEM images of test patterns of silver that were fabricated using μCP with hexadecanethiol, followed by selective chemical etching [102]. The SAMs protect the underlying substrates from dissolving by blocking the diffusional access of etchants. The ability to generate arrays of microstructures of coinage metals with controlled shapes and dimensions is directly useful in fabricating sensors and arrays of microelectrodes.

SAMs are prototypical self-assembled systems. They provide a convenient method for forming nanometer-thick "coatings" on solid substrates. Organic synthesis also makes it possible to incorporate different functional groups (with different physical, chemical, electrochemical, and biochemical properties) into and/or at the termini of the alkyl chain. As a result, SAMs themselves are excellent model systems for studies on wetting, adhesion, lubrication, corrosion, nucleation, protein adsorption, and cell attachment [103–105]. The coupling of SAMs with microcontact printing offers a powerful strategy for fabricating small, high-quality

patterns and structures with virtually no specialized equipment. Although the initial pattern is formed in SAMs, subsequent processes such as selective etching and deposition make μCP a convenient and versatile method for the formation of patterned microstructures of a wide variety of materials. Microfabrication based on μCP and SAMs offers a higher degree of control over the detailed, molecular-level structure of the interfaces than does photolithography. It can also be readily applied to types of patterning where photolithographic techniques simply fail, for example, patterning nonplanar surfaces [106]. We believe that μCP will become the major patterning technique in areas where cost or control of surface chemistry is the primary concern. Two issues remain to be solved before μCP can find applications in microelectronics: systems that form high quality SAMs on semiconductors must be developed; and the formation and distribution of defects in SAMs, especially under the conditions of chemical etching, must be understood.

3.3 Molecular Self-Assembly in the Solid State: Molecular Organic Crystals

The CA·M lattice is a useful starting point for crystal engineering because it predictably forms hydrogen-bonded substructures: tapes or rosettes (Figure 2). The triplet of hydrogen bonds that holds the components together is strong enough to generate these motifs reliably. We were able to rationalize each motif in model systems by identifying the molecular features responsible for promoting each motif. In particular, our clearest success has been in rationalizing general trends in the molecular arrangements *within these motifs* for cocrystals of *para*-substituted diphenylmelamines (**9**) and barbital (**10**) [107]. That is, we were able to control whether the molecules adopted a linear tape, a crinkled tape, or a rosette motif by altering the size of the substituents (Figure 12) [107].

Despite our successes, the potential of CA·M in crystal engineering may be limited. Several features of this system contribute to these limitations. First, growing diffraction-quality crystals in this series remains slow and difficult; in an ideal system, crystallization would be more straightforward. Second, the system does not tolerate polar substituents well. Third, the occurrence of polymorphism decreases the level of control that can be exercised in the system (Figure 13): complexities in packing due to conformational isomerism may be one of the biggest hurdles hindering the rational design of molecular crystals. In principle, each accessible conformation can pack as a separate crystalline phase. While the CA·M system has many attractive characteristics, it is probably too complex to serve as a basis for extensive studies at the current state of development of the field.

We have examined a second system based on 4,5-disubstituted 2-benzimidazolones (cyclic ureas, **11**). Although cyclic ureas were substantially simpler structurally than systems based on CA·M, the tape motif was less robust, and a number of nontape structures formed [108].

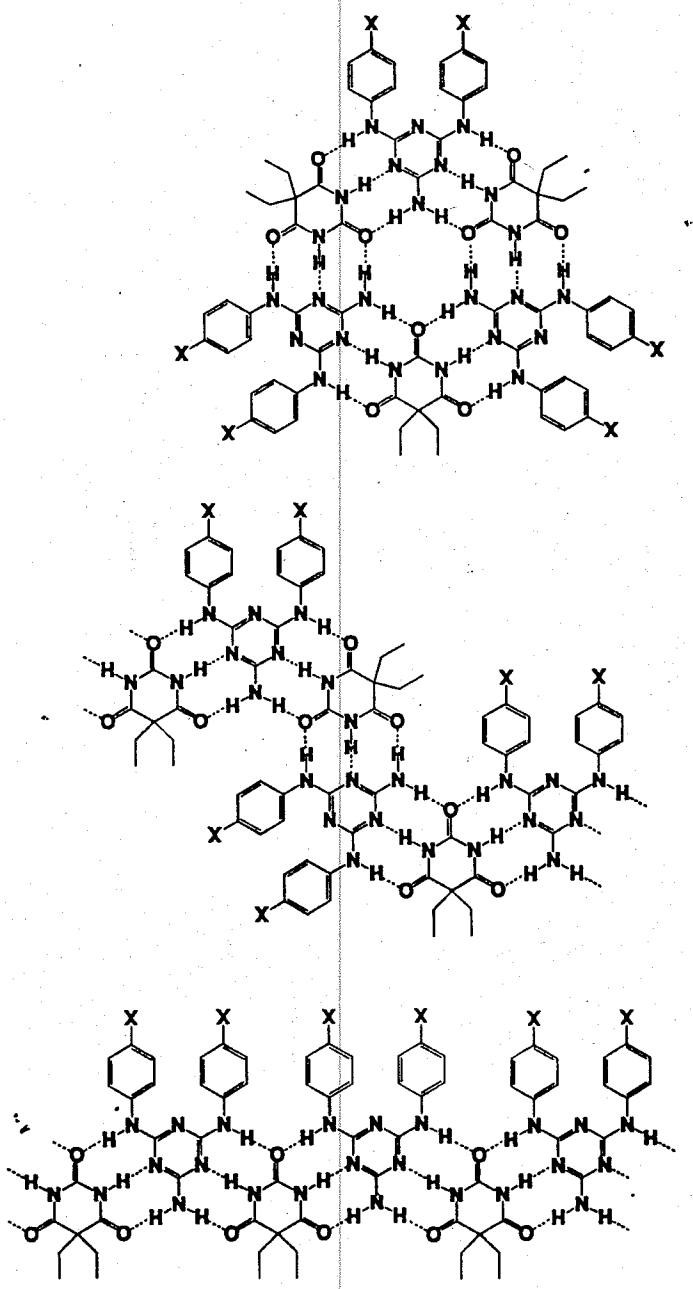

Figure 12 Illustration of three motifs – linear, crinkled, and rosette – that are based on CAM. The size of the para-substituent governs the motif that is formed

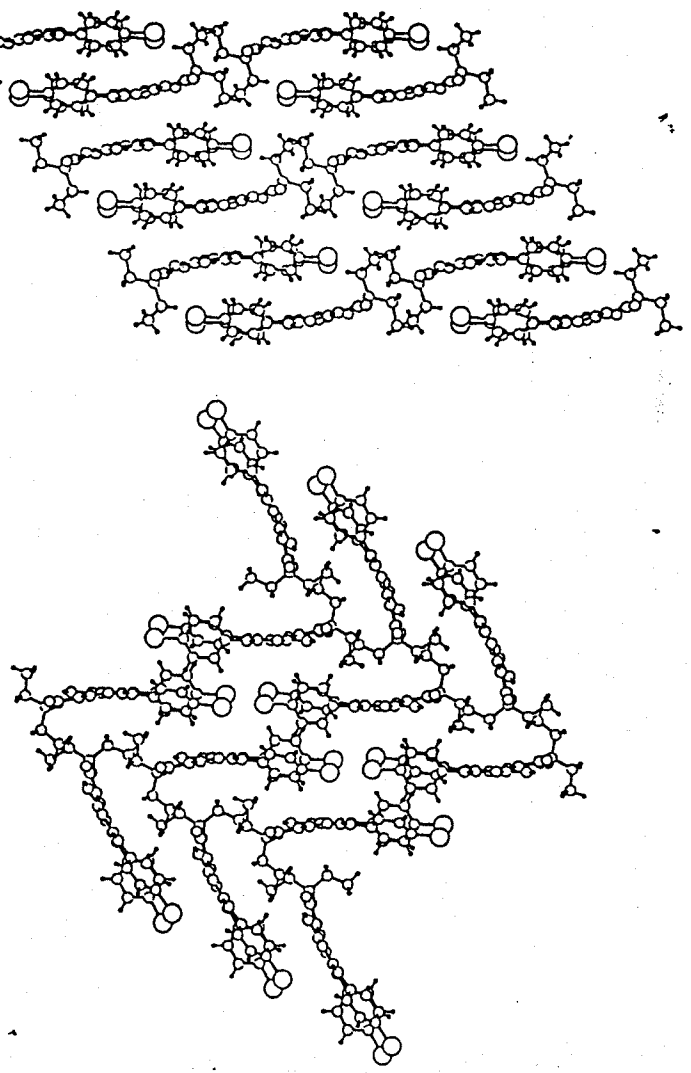

Figure 13 Single crystal X-ray structures of two polymorphic forms of the 1 : 1 cocrystal between diethylbarbital and bis-(*p*-bromophenyl)melamine

Among the classes of molecules able to form hydrogen-bonding-based tapes, the diketopiperazine (DKP) family now appears to be the most attractive [30]. The molecular packing in this system of crystals is less complex than systems based on CA·M or cyclic ureas, because there is only one possible tape. The locations of the 3,6-substituents seems to "protect" the secondary amide groups from interactions

with other amide groups, and thereby constrains the motif to one type of hydrogen-bond network.

More than 40 crystal structures of DKPs (**12**) have already been published [30]. Almost all of these DKPs form linear tapes that pack with their long axis parallel.

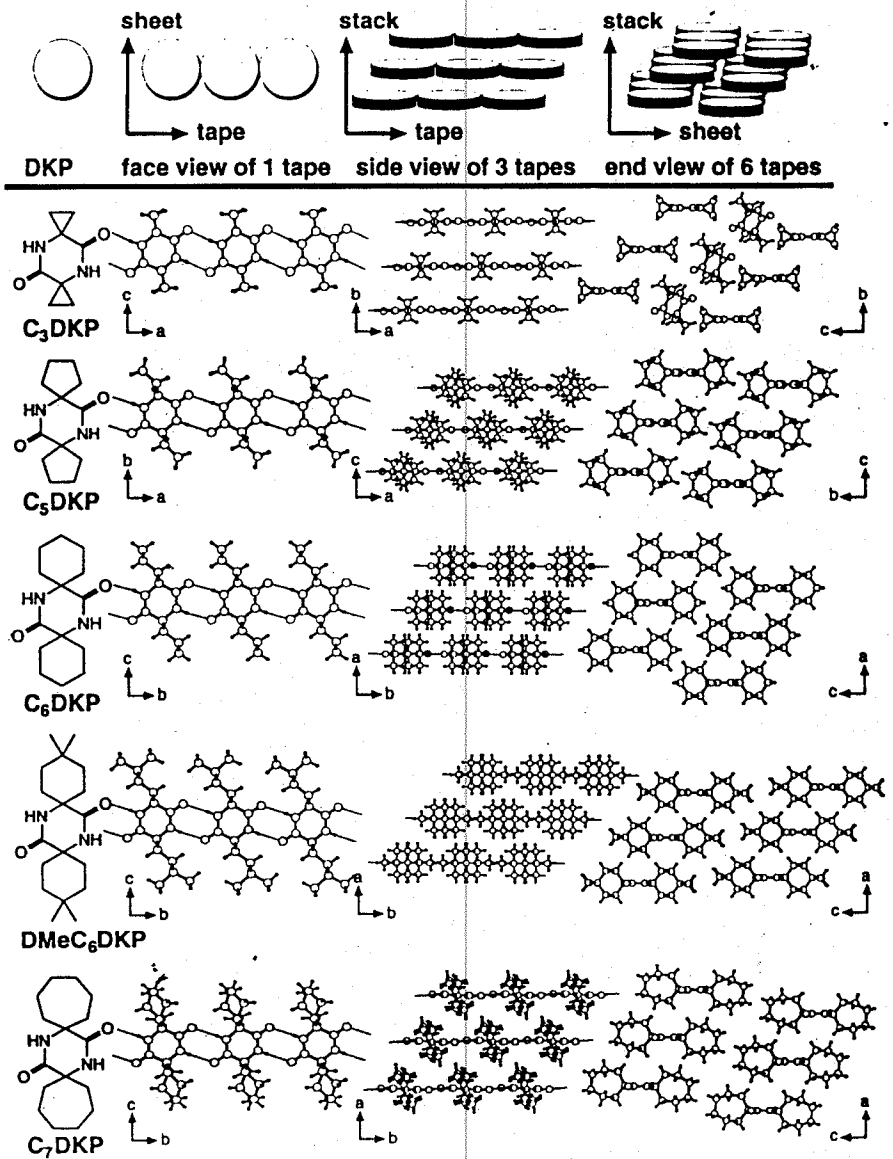

Figure 14 Crystal structures of four different DKP derivatives viewed in three different orientations. All form hydrogen-bonded tapes

The geometry of the tapes and their packing do not seem to depend strongly on the size, location, and (within some limitations) the type of substituent as is demonstrated in some of the crystals that we have analyzed (Figure 14) [109]. The robustness of the tape motif found in the crystal structures of the DKPs suggests that this system is an excellent platform for studying the packing arrangements of molecules in crystals.

The field of crystal engineering – designing crystals *de novo* based on molecular structures – is still in its prolonged infancy. DKPs do not have the generality to provide the basis for a broad range of different types of crystals, but it provides the most practical system that has been identified to date.

3.4 Mesoscale Self-Assembly

Mesoscopic self-assembly (MESA) is the assembly of *objects* into ordered arrays or units. We define an object as a body whose size is such that its properties can only be considered as those of a material: that is, as collections of many atoms. For example, proteins have a well-defined arrangement of atoms and known molecular weights; we consider them molecules. Colloids, nanotubes, and micron-sized structures fabricated from metals, ceramics, or polymers do not have precisely defined atomic arrangements or molecular weights; we consider them objects. The lower limit on the size of objects considered interesting for use in MESA is set by the upper limit of sizes of molecules that can be made in the laboratory or by nature; the upper limit on the size of the objects for MESA is set by the lower limit of objects that can be better or more easily assembled by the human hand or by machine [1,7]. The size range for the objects varies from several nanometers to centimeters: seven orders of magnitude. Included in this size regime are nanotubes, colloids, cells, transistors, computer chips, bearings, and micromotors, these objects are interesting in fields ranging from biology to microelectronics [110,111].

Mesoscale self-assembly is a new area of research; Figure 15 shows the most notable of these systems [35,112–115]. Gold colloids 13 nm in diameter were assembled into a disordered array based on complementary strands of DNA (Figure 15A) [116]. The colloids were covered in one of two different SAMs terminated in different, noncomplementary DNA sequences. When a soluble linker complementary to both strands was added to an aqueous solution of two colloids the colloids became cross-linked due to DNA duplex formation. The array that formed is not well-characterized but is believed to be densely packed. An example of MESA using micron-scale objects is the electrostatic assembly of gold cylinders onto a gold surface patterned with two different alkanethiols (Figure 15B) [117]. The cylinders are covered with a SAM terminated in $-PO_3H_2$. The cylinders selectively assembled onto regions of a patterned gold coated silicon wafer bearing a SAM terminated in $-NMe_3^+$ groups; the cylinders did not assemble onto regions terminated in $-CO_2^-$.

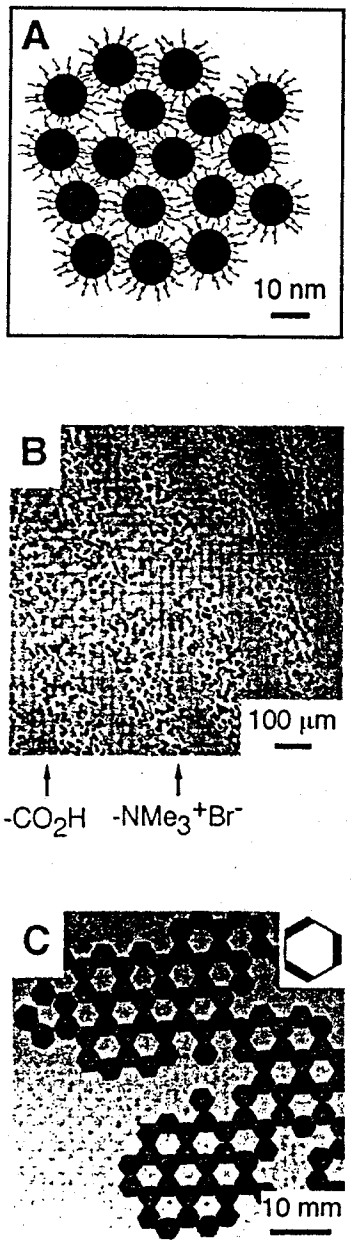

Figure 15 Three examples of mesoscale self-assembly spanning the range from nanometers to millimeters. (A) Gold colloids 13 nm in diameter that are coated with a DNA terminated SAM. The colloids flocculate when a strand of DNA, whose ends are complementary to the DNA on the SAM, is added. (B) Gold cylinders that are 10 μm in diameter, 10 μm high, and are coated with a SAM terminated in PO_3H_2 selectively assemble onto regions on a gold surface where the SAM is terminated in $-NMe_3^+$ and avoid those regions where the SAM is terminated in $-CO_2H$. (C) The hexagons shown assemble due to lateral capillary forces. In the inset the bold sides indicate hydrophobic faces and the thin sides indicate hydrophilic faces. The hexagons are floating at the perfluorodecalin–water interface. The perfluorodecalin wets the hydrophobic faces; when two hydrophobic sides are in close proximity the free energy of the system is lowered and the objects remain in contact

A promising new system for MESA on the millimeter-scale is the assembly of PDMS objects at the water–perfluorodecalin (PFD) interface (Figure 15C) [33]. PDMS objects ($\rho = 1.05\,g\,cm^{-3}$) float at the interface between PFD ($\rho = 1.90\,g\,ml^{-1}$) and water ($\rho = 1.00\,g\,ml^{-1}$); lateral capillary forces between the objects result in self-assembly. By controlling the hydrophobicity of the sides, we can direct the assembly of the objects into different arrays. PFD wets the hydrophobic sides and forms menisci; the menisci are high in energy because they increase the PFD–water surface area [118–120]. The decreased size of the menisci when two hydrophobic sides come into contact lowers the free energy of the system and holds the objects together (Figure 16A). Water wets the hydrophilic sides. The magnitude of this wetting is smaller than when PFD wets hydrophobic faces; thus, two hydrophilic faces are only weakly attractive toward each other (Figure 16B). Hydrophobic and hydrophilic sides exhibit a repulsive interaction due to the increase in perfluorodecalin–water surface area when the two sides come into contact (Figure 16C).

Self-assembly of millimeter-scale objects at the PFD–water interface based on lateral capillary forces is attractive for several reasons. First, the objects are easy to fabricate. Second, even though PDMS is naturally hydrophobic it can be rendered hydrophilic by oxidation in an oxygen plasma [121]. Third, we can control which sides remain hydrophobic by covering them with tape before oxidation; exposed sides become hydrophilic. Fourth, capillary forces are well understood from a theoretical point of view and modeling the assembly process should be possible [119,120]. Fifth, capillary forces are long range and objects are attracted to one another at distances up to several times their heights. Sixth, the assembly is rapid and reversible, a typical assembly is done in less than 30 min. We use this system to illustrate some of the general ideas and issues of MESA in the next section.

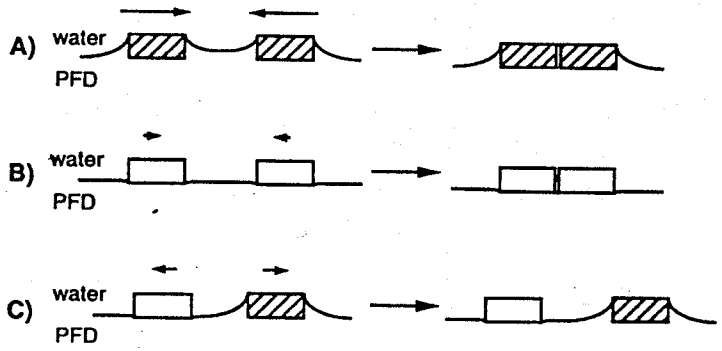

Figure 16 (A) Two hydrophobic objects are strongly attracted to one another due to the large menisci formed when PFD wets the hydrophobic sides of the objects. (B) Two hydrophilic objects are only weakly attracted to one another due to the small menisci formed when water wets the hydrophilic sides of the objects. (C) A hydrophobic object is repelled by a hydrophilic object

The current range of structures that can be made using MESA is limited. From the nanometer to the micron size range it is exceedingly difficult, if not impossible, to design and build complex three-dimensional structures with differentiated recognizing elements. Most of the work in MESA has been limited to making two- and three-dimensional close-packed arrays of colloids [116,122,123]. Several techniques exist on the micron to the millimeter size range that allow fabrication of complex three-dimensional objects, for example: photolithography, soft lithography, and molding. At this point we can assemble a variety of simple arrays, in the future we intend to assemble large, complex arrays.

(a) Experimental issues

In the following paragraphs we will discuss some of the important problems and issues that are faced in designing a MESA system. Some of the most important experimental issues include the choice of material, design and fabrication of the objects, forces, and how the objects are assembled.

Choice of material In the case of the two-dimensional array shown in Figure 15C, the material used to make the objects was chosen primarily based on two criteria: first, the objects had to have a density between that of water and perfluorodecalin, and second, the objects had to have sides that could be selectively rendered hydrophobic or hydrophilic. PDMS fulfills these criteria in addition to being easy to fabricate into many shapes. In other systems a consideration of the Young's modulus, durability, electrical conductivity, hardness, and the range of shapes that can be fabricated may be important. The choice of material in the nanometer to micron size range is currently limited by the method of fabrication.

Design and fabrication of the objects The design and fabrication of the individual objects are two important and closely related problems in this area. Useful techniques for fabrication include the combination of photolithography and electrodeposition of metals (this technique was employed to make the objects in Figure 15B), the use of a mold (this technique was employed to make the objects in Figure 15C), soft lithography, synthesis of colloids, and reactive ion etching. Improved techniques will be needed in the future to make complex objects on a nanometer and micron scale.

In order to form complex arrays, the sides of the objects must be differentiated from one another; without this differentiation only close- or loosely-packed arrays can form. For example, in Figure 17A all of the sides of the hexagons are hydrophobic and a close packed array is formed. Figures 17B and 17C show two examples where the sides of the hexagons are differentiated; different open arrays were assembled with these hexagons. Although the formation of close-packed arrays is interesting and can give important information about MESA, the ability to form a

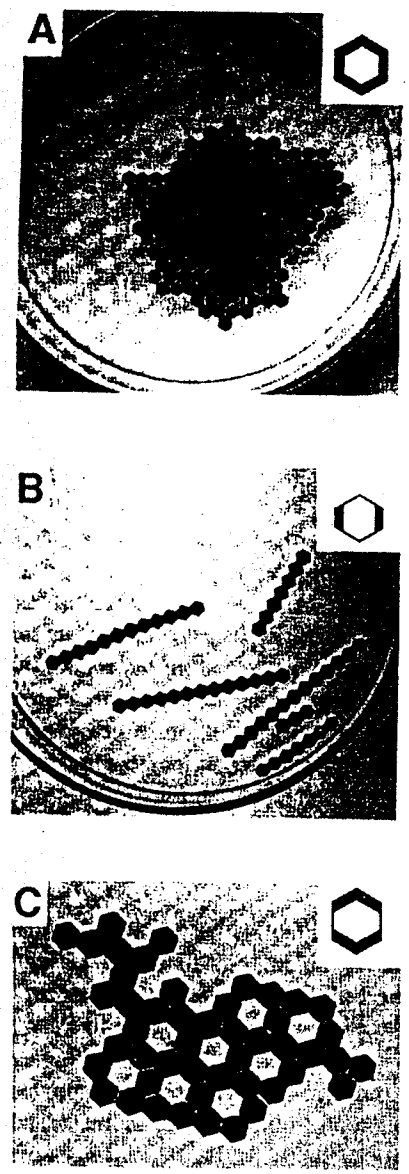

Figure 17 Three examples of two dimensional self-assembly based on one structure, hexagons. In the insets the bold sides indicate hydrophobic faces and the thin sides indicate hydrophilic faces. The hexagons are floating at the perfluorodecalin–water interface. The array shown in (A) results when all the sides are equivalent and hydrophobic; (B) and (C) show two of the arrays possible when the sides are differentiated

variety of arrays by differentiating the sides of the objects will allow us to discern the basic rules of MESA. In our system this problems is solved by physically protecting sides of the hexagons before the oxidation, for smaller systems new techniques may need to be developed.

Forces An important choice in MESA is that of the inter-object forces to be used. The range of forces that can be used has not been established; we surmise that those

Forces Appropriate to use in Mesoscopic Self-Assembly (MESA)

Capillary
Surface
Ferro- and paramagnetic
Hydrophobic
Electrostatic
Van der Waals
Biospecific
(DNA duplex, protein-ligand)
Metal-ligand
Light
Gravitational
Shear
Electrophoretic
Diaphoretic
Wave
Centrifugal

Figure 18 Examples of interactions that may find uses in mesoscale self-assembly. Some interactions can be used to pull objects together that are separated by distances greater than 100 nm, while other forces are strong over short separations (less than 100 nm) but much weaker or nonexistent over longer separations

forces listed in Figure 18 may prove to be useful. The most successful examples that we have achieved are based on lateral capillary forces (Figure 15C). Lateral capillary forces are particularly effective because we can control their strength by altering the height of the object and the hydrophobicity of the sides. Another attractive feature of lateral capillary forces is that they are sufficiently attractive between objects separated by distances equal to several times their heights and are of sufficient magnitude to hold the objects together.

Assembly of objects In the assemblies shown in Figure 15C and Figure 17, the objects were agitated by shaking in a circular motion in the plane of the perfluorodecalin/water interface. The objects at the edge of the dish have more kinetic energy than those in the center of the dish; this distribution in kinetic energy results in a non-Boltzmann distribution of energy. A variety of other methods for supplying energy for the self-assembly process are conceivable, these include: heating, sonication, microwave heating, and vibrational agitation. These methods of supplying energy may result in a non-Boltzmann distribution of energy among the objects, the detailed thermodynamic properties need to be worked out. Two future

critical problems to solve are the duration over which energy is supplied to the system and the development of improved methods for characterization of the final array. Methods for characterizing the arrays include TEM, SEM, diffraction patterns, and optical microscopy. Physical rules describing the association and dissociation processes remain to be established.

3.5 Issues in Theory

(a) Methods that calculate entropy and enthalpy for molecular systems

Computations should reliably predict stabilities of complexes in terms of common quantities – enthalpy and entropy – to be broadly useful to physical organic chemists interested in self-assembly. There are extensive reviews on the use of potentials in calculating these quantities [124,125]. Some of the general issues are the following. Enthalpy can be determined accurately from quantum mechanics (QM), but the method is limited to a few atoms: far below the number of interest to the supramolecular chemist. Enthalpy is approximated by empirical potentials (EP). These EP are accurate in some systems where parameterization is of particular high quality, but poor in others, because EP are not easily transferable between systems. EP are currently the only way to study the dynamics of atomistic models of aggregates the size of those discussed in this review. Entropy is determined by evaluating the partition function for vibrational, rotational, and translational degrees of freedom (DOF). Normally, only the vibrational contribution to entropy can be calculated for *atomistic* models of modest flexibility; calculating the contributions to entropy from rotational and translational entropy is prohibitively time consuming. Most popular force fields based on EP are adequate for simple organic compounds; they have been, however, developed primarily for use with biological systems, and may not be appropriate for other problems (for example, crystal engineering) [126].

(b) Increasing the efficiency of simulations

The time-dependent mechanism of molecular interactions can be studied, in principle, by solving Newton's equations of motion using a variety of molecular dynamics methods [127]. Simulating the process of aggregation, however, remains an intractable problem for computational supramolecular chemistry. The root of the problem is the relatively short time scale accessible by simulations. Two factors, other than the available computational power, contribute to this limitation: the number of atoms, particularly those systems where solvent is included; the fastest motion in the system (e.g. bond stretches): dynamics algorithms must include the fastest motion in its calculations to be stable energetically. Currently, simulations on the order of nanoseconds are considered cutting edge; this value is far too short to simulate accurately many (and perhaps all) systems of interest.

Some of the new methods that are being developed to reduce the amount of calculations are the following.

- Those that eliminate the high frequency motions by grouping many atoms in a system into rigid or flexible entities, and thereby allow larger time steps (spanning several orders of magnitude) in the simulation [128–130].
- Those that model the effects of solvent without explicitly including each molecule of solvent in the calculations. One such strategy is based on Brownian motion, and has been used to simulate events that happen on the millisecond time scale (but at the expense of much atomistic detail): for example, the diffusion of a ligand into the active site of a protein [131] and the supercoiling of DNA [130]. A second strategy is the handling of the effects of solvent on long range electrostatics interactions by solving the Poisson–Boltzmann equation [132,133].

Many of these methods are being tested on problems in biochemistry (e.g. protein–ligand, and DNA–protein interactions), and their applications to problems in supramolecular chemistry should be straightforward.

(c) Surrogates for ΔG

It is impractical to calculate the complete thermodynamic cycle for the formation of self-assembled molecular systems of the size and complexity of those discussed in this review. Methods that "mutate" the system from one kind to another are not applicable to such large systems [134]. Surrogates for relative stabilities, therefore, must be developed. Two such methods that we have developed are the following.

Deviation from planarity (DP) The values of *DP* measure the extent to which the components of the CA•M motif are out of plane with each other relative to a coplanar geometry that represents a minimum in free energy (Figure 19). The higher the value of *DP*, the more unstable the complex. For aggregates based on CA•M, we have found that *DP* correctly ranks the order of stabilities for a variety of different complexes [55,56], and for conformational isomers of a single aggregate [54]. Values of *DP* are typically calculated from an ensemble of conformations from molecular dynamics simulations. In this way, the effects of enthalpy and *entropy* are implicitly included in the value of *DP*. We have found that *DP* is sensitive to the effects of solvent and conformational flexibility. It remains to be established, however, whether *DP* can be an effective surrogate for ΔG in other systems.

HB/($N-1$) The ratio of the number of hydrogen bonds in the system (*HB*) to the number of particles (N), is a convenient and simple first approximation to predicting stability in systems based on CA•M [28,49]. This simple ratio is a coarser metric for ranking stabilities than *DP*, but it does not involve the complexities of setting up an atomistic simulation. The range of systems amenable to *HB*/($N-1$) is, however,

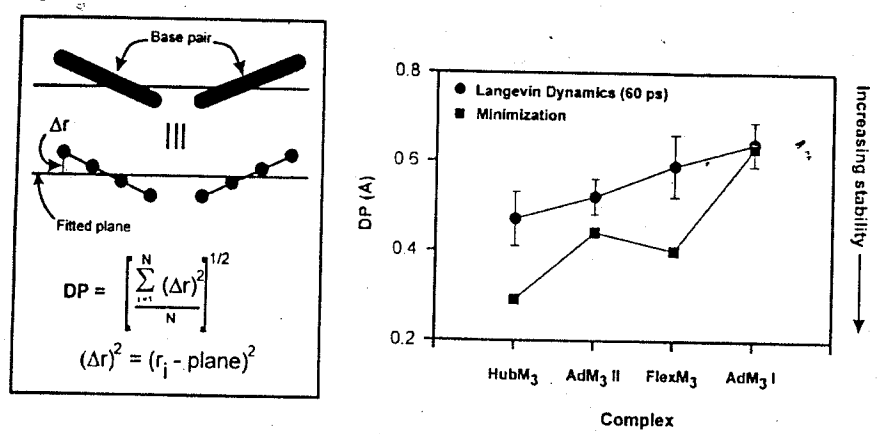

Figure 19 The definition of DP (left) and the results for several complexes based on CA•M (right). Hub(M)$_3$ and Flex(M)$_3$ are discussed in the section on soluble aggregates; Ad(M)$_3$ I and Ad(M)$_3$ II are similar to Hub(M)$_3$, the primary difference is that adamantane instead of benzene is the central hub in the tripod [55]. The results from molecular dynamics (circles) and minimization calculations (squares) are shown

limited: that is, for any two different complexes, we assume that $\Delta\Delta H$ is dominated by hydrogen bonds, and the $\Delta\Delta G$ of solvation is close to 0.

(d) Specific computational issues

We have discussed some of the broader issues facing computational supramolecular chemistry, and we will now discuss some of the specific computational issues that we have experienced in the areas explored in this review.

Soluble aggregates New computational tools for assembling supramolecular structures are needed. We have been frustrated by the difficulty of manipulating many molecules in 3D into a plausible aggregate. As we have discussed, CPK models were not useful beyond a basic conceptual stage; new computational tools that easily manipulate many molecules into structures such as the tetrahedral aggregate shown in Figure 7 would be very useful. New and efficient theories for predicting relative stabilities that are generally applicable to systems other than those based on hydrogen bonds, or CA•M, are needed. One question that we have not addressed is the transferability of methods such as *DP* or $HB/(N-1)$ to systems other than those for which they were developed.

SAMs Simulations involving SAMs are particularly computationally demanding because the rearrangement of molecules for such close packed systems is slow on the sub-nanosecond time scale [135]. These simulations have been useful to us,

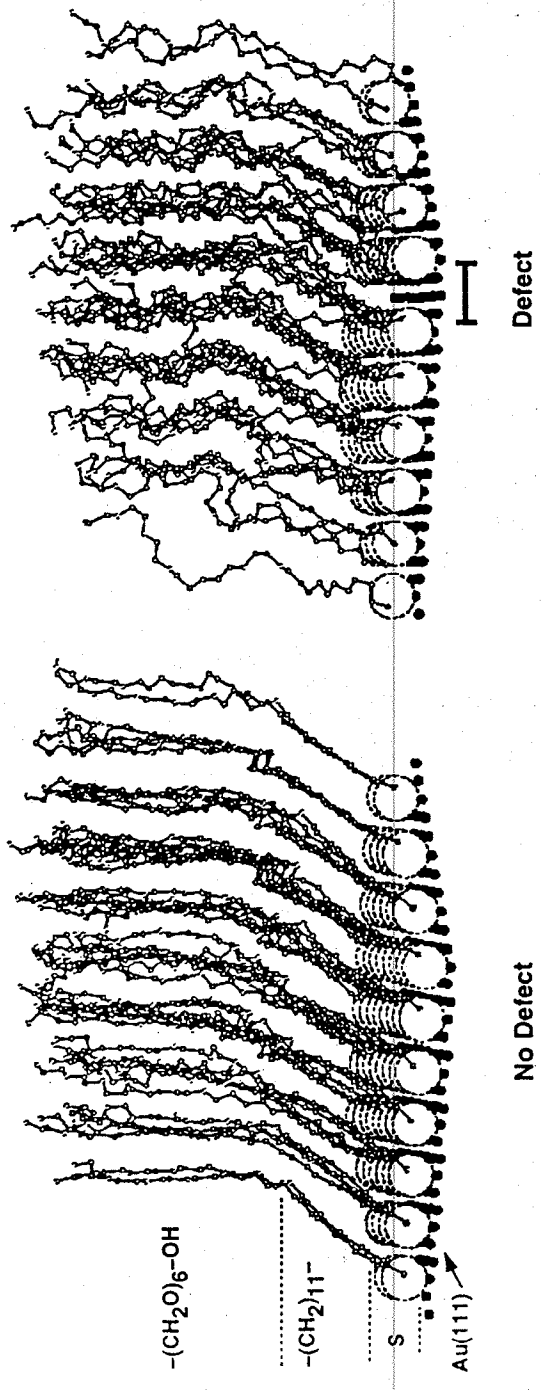

Figure 20 The last frames (representative) of two 600 ps simulations of a self-assembled monolayer (SAM) on Au(111). When a defect was introduced by shifting roughly half of the chains to the next interstitial site on the Au(111) surface (this resulted in the loss of four chains in the system below), the chains reoriented to a helical conformation to fill the voids caused by the defect. A 1.5 nm layer of water was placed on top of the SAM, and the computations were carried out in the presence of 2-D periodic boundaries to mimic an infinite SAM. Only the non-water molecules and atoms of the primary system are shown for clarity

nevertheless, in suggesting new ways of thinking about SAMs (Figure 20) [136]; the large computational efforts involved, however, have limited such simulations from being a routine part of our studies.

Crystal engineering A particularly challenging problem in supramolecular chemistry is predicting the crystalline packing arrangement of a molecule given only the geometrical and chemical information of a single molecule [137–143]. There are two main problems for computations. First, molecules can pack in an astronomical number of different ways, and searching through these arrangements is computationally impossible. Second, many of these crystalline arrangements can be similar in energy – differences on the order of 2 kcal mol^{-1} – and it is unlikely that present-day empirical force fields can accurately separate two polymorphs [140]. One strategy that we have successfully tested and implemented is to reduce the magnitude of the dimensionality problem by constraining the molecules to form hydrogen-bonded tapes. The hydrogen bond is a particularly useful type of constraining force as we and others have reviewed previously [30,144].

We were able to develop some simple rules in predicting the packing of molecules based on CA•M in one dimensional tapes, but not for predicting the three-dimensional packing of these tapes [98,107,145–148]. Conformational polymorphism due to the diphenyl rings, in addition, increased the complexity of the problem in the CAM system. We have found that crystal structures based on diketopiperazines (DKP) are simpler to predict and rationalize than our previous systems, both from observations of existing structures, and from computational methods [30,109].

Predicting the packing of organic crystals is not a completely unachievable goal, however: strategies exist to yield tractable computations by studying systems like DKP that can be predisposed to form tapes. We have used simulated annealing Monte Carlo methods [137] in concert with procedures that restrict the search to those molecular arrangements that have reasonable hydrogen bonds, to predict crystalline structures that compare well with those from experiment (Figure 21) [136].

One area that has not been extensively explored with computations, however, is the nucleation, or kinetics, of crystalline growth. The process of growing crystals is typically the rate limiting step in our studies in crystal engineering.

Mesoscale self-assembly We have not yet modeled MESA by computer, but with the wealth of experimental results we are in a position to develop believable computer simulations calibrated by experiment. The force of attraction between the objects is well understood mathematically in a number of cases [33,120] and in some systems it may be possible to measure these forces experimentally [149]. Some of the problems encountered in modeling molecular systems will also be encountered in modeling MESA. For example, finding global rather than local minima, the availability of computer time limiting how long the assembly can be modeled, and constructing potential functions for interactions that have not been determined

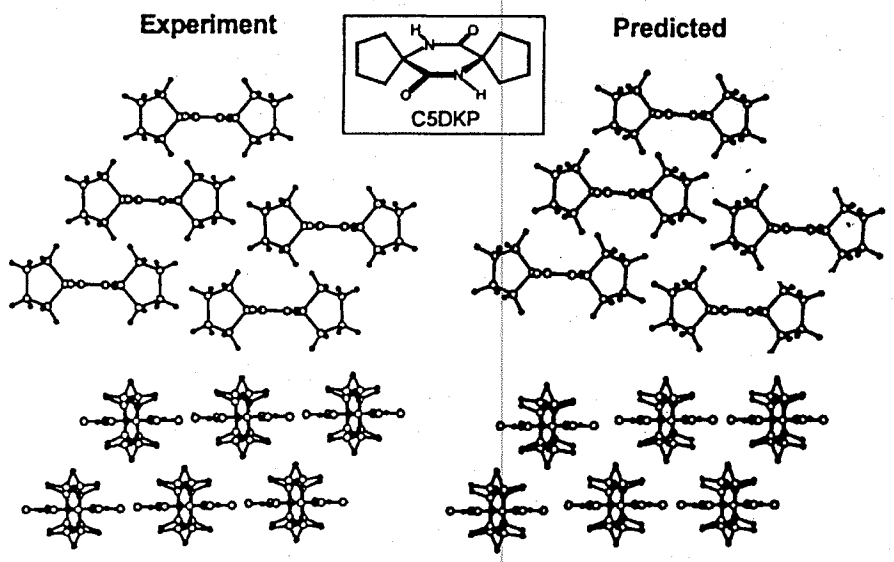

Figure 21 The experimental and predicted crystal structures for C_5DKP

experimentally are all important issues. Computer models already exist, however, that use simple geometric shapes and interactions to build arrays and optimizing these models for MESA may be possible.

The distribution of energy (supplied by shaking, sonication, or heating) in the system and the definition of entropy in MESA may be challenging. The distribution of kinetic energy among the objects will not necessarily follow Boltzmann's distribution and new thermodynamic descriptions will need to be developed. The two-dimensional self-assembly shown in Figure 17 is a good example of a MESA system where the distribution of energy is complex. The objects are agitated in a circular motion and the objects on the outer edge of the array have more kinetic energy than those in the center of the array. Entropy is an important part of all systems, but we have little knowledge of how to model this quantity.

4. SUMMARY AND CONCLUSIONS

We have described our recent work on four different self-assembling systems: self-assembly in solution based on the hydrogen-bonded CA•M rosette, self-assembly in the organic solid state using hydrogen-bonds, self-assembly of monolayers of alkanethiolates on gold, and self-assembly of mesoscale objects floating at the water–PFD interface. We have not yet succeeded in preparing arbitrarily structurally or functionally complex aggregates, although the formation of SAMs on gold shows excellent promise in this regard (mesoscale self-assembly is not yet sufficiently

developed to draw conclusions). Many important problems remain to be addressed in each of these areas. In molecular self-assembly, the lack of convenient computational tools for the construction and evaluation (enthalpic and entropic) of self-assembled structures and the difficulty of preparing self-assembled structures in water using the hydrophobic effect are two important issues to addfess. For crystal engineering, two of the most important current experimental difficulties are the occurrence of polymorphs and the growth of X-ray quality crystals. Computationally, the most important issue to address is the development of methods that correctly predict crystal structure from molecular structure. For SAMs to find more diverse use in areas like microelectronics, the development of methods for forming them on semiconductors and the control of the number and nature of defects in the SAMs are critical issues. For mesoscale self-assembly, improved methods for the fabrication and selective functionalization of micron sized objects will be of critical importance.

These systems have taught several lessons relevant to future studies in self-assembly. What characteristics should be considered in the design of a self-assembling system? First, the molecules or objects should be designed such that a single motif forms in every case (e.g. CA•M rosette, hydrogen bonded tapes, close packed hexagonal array of alkanethiolates on gold, and mesoscale hydrophobic side–hydrophobic side interactions). Second, the strength of the different interactions used should be of different orders of magnitude. Third, the self-assembled structures should bear several selectively functionalizable sites that do not interfere with the assembly process. Self-assembly based on hydrogen bonds in solution and the solid state meets (partially) the first criteria, but does not meet the second or the third. Specifically, the similar magnitudes of the favorable enthalpies of formation of the hydrogen bonds and the unfavorable conformational, rotational, and translational entropies of aggregation have made it difficult to progress to more complex aggregates. In contrast, SAMs meet all three of these criteria; they form every time, the strong Au–S bond and the weaker interchain packing determine the overall structure whereas the easily synthetically varied headgroup determines the properties of the interface. We believe that mesoscopic self-assembly of PDMS objects at the perfluorodecalin–water interface is another system that meets these three criteria and that this system will become as versatile as SAMs on gold.

5. ACKNOWLEDGMENTS

We are grateful to the NSF (CHE-91-22331), and ONR/DARPA for financial support of the work described in this review. L.I. and N.B. would like to thank, respectively, the NIH and DOD for postdoctoral and doctoral fellowships.

6. REFERENCES

1. G. M. Whitesides, J. P. Mathias and C. T. Seto, *Science*, **254**, 1312 (1991).
2. J.-M. Lehn, *Science*, **260**, 1762 (1993).

3. J.-M. Lehn, *Angew. Chem. Int. Ed. Engl.*, **27**, 89 (1988).
4. D. J. Cram, *Angew. Chem. Int. Ed. Engl.*, **27**, 1009 (1988).
5. C. J. Pederson, *Angew. Chem. Int. Ed. Engl.*, **27**, 1021 (1988).
6. E. L. Shakhnovich, V. Abkevich and O. Ptitsyn, *Nature*, **379**, 96 (1996).
7. A. Klug, *Angew. Chem. Int. Ed. Engl.*, **22**, 565 (1983).
8. D. Voet and J. G. Voet, *Biochemistry*, John Wiley, New York, 1995.
9. M. R. Ghadiri, J. R. Granja, R. A. M. Milligan, D. E. McRee and N. Khazanovich, *Nature*, **366**, 324 (1993).
10. J.-P. Sauvage, *Acc. Chem. Res.*, **23**, 319 (1990).
11. S. C. Zimmerman, F. Zeng, D. E. C. Reichert and S. V. Kolotuchin, *Science*, **271**, 1095 (1996).
12. J. Kang and J. Rebek Jr., *Nature*, **382**, 239 (1996).
13. S. Anderson, H. L. Anderson and J. K. M. Sanders, *Acc. Chem. Res.*, **26**, 469 (1993).
14. R. G. Chapman and J. C. Sherman, *J. Am. Chem. Soc.*, **117**, 9081 (1995).
15. D. Philp and J. F. Stoddart, *Angew. Chem. Int. Ed. Engl.*, **35**, 1154 (1996).
16. T. Beissel, R. E. Powers and K. N. Raymond, *Angew. Chem. Int. Ed. Engl.*, **35**, 1084 (1996).
17. J. Rebek Jr., *Chem. Soc. Rev.*, **96**, 255 (1996).
18. J.-C. Chambron, C. Dietrich-Buchecker and J.-P. Sauvage, in *Comprehensives Supramolecular Chemistry* (Series eds J.-M. Lehn, J. L. Atwood, J. E. D. Davies, D. D. MacNicol and F. Vögtle), Volume 9 (eds J.-P. Sauvage and M. W. Hosseini), Pergamon, New York, 1996, pp. 43–83.
19. P. N. W. Baxter, in *Comprehensive Supramolecular Chemistry* (Series eds J.-M. Lehn, J. L. Atwood, J. E. D. Davies, D. D. MacNicol and F. Vögtle), Volume 9 (eds J.-P. Sauvage and M. W. Hosseini), Pergamon, New York, 1996, pp. 165–211.
20. T. Kunitake, in *Comprehensive Supramolecular Chemistry* (Series eds J.-M. Lehn, J. L. Atwood, J. E. D. Davies, D. D. MacNicol and F. Vögtle), Volume 9 (eds J.-P. Sauvage and M. W. Hosseini), Pergamon, New York, 1996, pp. 351–406.
21. M. Fujita, in *Comprehensive Supramolecular Chemistry* (Series eds J.-M. Lehn, J. L. Atwood, J. E. D. Davies, D. D. MacNicol and F. Vögtle), Volume 9 (eds J.-P. Sauvage and M. W. Hosseini), Pergamon, New York, 1996, pp. 253–282.
22. A. Reichert, H. Ringsdorf, P. Schuhmacher, W. Baumeister and T. Scheybani, in *Comprehensive Supramolecular Chemistry* (Series eds J.-M. Lehn, J. L. Atwood, J. E. D. Davies, D. D. MacNicol and F. Vögtle), Volume 9 (eds J.-P. Sauvage and M. W. Hosseini), Pergamon, New York, 1996, pp. 313–350.
23. D. H. Lee and M. R. Ghadiri, in *Comprehensive Supramolecular Chemistry* (Series eds J.-M. Lehn, J. L. Atwood, J. E. D. Davies, D. D. MacNicol and F. Vögtle), Volume 9 (eds J.-P. Sauvage and M. W. Hosseini), Pergamon, New York, 1996, pp. 451–481.
24. J. R. Fredericks and A. D. Hamilton, in *Comprehensive Supramolecular Chemistry* (Series eds J.-M. Lehn, J. L. Atwood, J. E. D. Davies, D. D. MacNicol and F. Vögtle), Volume 9 (eds J.-P. Sauvage and M. W. Hosseini), Pergamon, New York, 1996, pp. 565–594.
25. X. Wang, M. Simard and J. D. Wuest, *J. Am. Chem. Soc.*, **116**, 12119 (1994).
26. B. Olenyuk, J. A. Whiteford and P. J. Stang, *J. Am. Chem. Soc.*, **118**, 8221 (1996).
27. W. T. S. Huck, F. C. J. M. van Veggel and D. N. Reinhoudt, *Angew. Chem. Int. Ed. Engl.*, **35**, 1213 (1996).
28. E. E. Simanek, M. Mammen, D. M. Gordon, D. N. Chin, J. P. Mathias, C. T. Seto and G. M. Whitesides, *Tetrahedron*, **51**, 607 (1995).
29. G. M. Whitesides, E. E. Simanek, J. P. Mathias, C. T. Seto, D. N. Chin, M. Mammen and D. M. Gordon, *Acc. Chem. Res.*, **28**, 37 (1995).
30. J. C. MacDonald and G. M. Whitesides, *Chem. Rev.*, 94, 2383 (1994).
31. G. M. Whitesides, *Sci. Am.*, **273**, 146 (1995).

32. G. M. Whitesides and P. E. Laibinis, *Langmuir*, **6**, 87 (1990).
33. N. Bowden, A. T. Terfort, J. Carbeck and G. M. Whitesides, *Science*, **276**, 233 (1997).
34. A. Terfort and G. M. Whitesides, *Adv. Mater.*, **10**, 470 (1998).
35. A. Terfort, N. Bowden and G. M. Whitesides, *Nature*, **386**, 162 (1997).
36. K. C. Nicolaou, F. P. J. T. Rutjes, E. A. Theodorakis, J. Tiebes, M. Sato, and E. Untersteller, *J. Am. Chem. Soc.*, **117**, 10252 (1995).
37. Y. Kishi, *Pure Appl. Chem.*, **61**, 313 (1989).
38. A. E. Eschenmoser and C. Wintner, *Science*, **196**, 1410 (1977).
39. R. B. Woodward, *Pure Appl. Chem.*, **33**, 145 (1973).
40. C. T. Seto and G. M. Whitesides, *J. Am. Chem. Soc.*, **112**, 6409 (1990).
41. J. P. Mathias, E. E. Simanek and G. M. Whitesides, *J. Am. Chem. Soc.*, **116**, 4326 (1994).
42. C. T. Seto and G. M. Whitesides, *J. Am. Chem. Soc.*, **113**, 712 (1991).
43. C. T. Seto, J. P. Mathias and G. M. Whitesides, *J. Am. Chem. Soc.*, **115**, 1321 (1993).
44. C. T. Seto and G. M. Whitesides, *J. Am. Chem. Soc.*, **115**, 1330 (1993).
45. C. T. Seto and G. M. Whitesides, *J. Am. Chem. Soc.*, **115**, 905 (1993).
46. J. P. Mathias, E. E. Simanek, C. T. Seto and G. M. Whitesides, *Angew. Chem. Int. Ed. Engl.*, **32**, 1766 (1993).
47. J. P. Mathias, C. T. Seto, E. E. Simanek and G. M. Whitesides, *J. Am. Chem. Soc.*, **116**, 1725 (1994).
48. J. P. Mathias, J. A. Zerkowski, C. T. Seto, E. E. Simanek and G. M. Whitesides, *J. Am. Chem. Soc.*, **116**, 4316 (1994).
49. M. Mammen, E. E. Simanek and G. M. Whitesides, *J. Am. Chem. Soc.*, **118**, 12614 (1996).
50. M. Mammen, E. I. Shakhnovich and G. M. Whitesides, *J. Org. Chem.*, **53**, 3168 (1998).
51. E. E. Simanek, M. I. M. Wazeer, J. P. Mathias and G. M. Whitesides, *J. Org. Chem.*, **59**, 4904 (1994).
52. X. Cheng, Q. Gao, R. D. Smith, E. E. Simanek, M. Mammen and G. M. Whitesides, *Rapid Comm. Mass Spec.*, **9**, 312 (1995).
53. X. Cheng, Q. Gao, R. D. Smith, E. E. Simanek, M. Mammen and G. M. Whitesides, *J. Org. Chem.*, **61**, 2204 (1996).
54. D. N. Chin, E. E. Simanek, X. Li, M. I. M. Wazeer and G. M. Whitesides, *J. Org. Chem.*, **62**, 1891 (1997).
55. D. N. Chin, D. M. Gordon and G. M. Whitesides, *J. Am. Chem. Soc.*, **116**, 12033 (1994).
56. X. Li, D. N. Chin and G. M. Whitesides, *J. Org. Chem.*, **61**, 1779 (1996).
57. M. Mammen, E. I. Shakhnovich and G. M. Whitesides, *J. Org. Chem.*, **63**, 3821 (1998).
58. L. Isaacs and G. M. Whitesides, unpublished results.
59. A. Ulman, *Introduction to Ultra Thin Organic Films: From Langmuir–Blodgett to Self-Assembly*, Academic Press, Boston, 1991.
60. C. D. Bain and G. M. Whitesides, *Angew. Chem. Int. Ed. Engl.*, **28**, 506 (1989).
61. L. H. Dubois and R. G. Nuzzo, *Annu. Rev. Phys. Chem.*, **43**, 437 (1992).
62. E. Delamarche, B. Michel, H. A. Biebuyck and C. Gerber, *Adv. Mater.*, **8**, 719 (1996).
63. J. Xu and H.-L. Li, *J. Coll. Interf. Sci.*, **176**, 138 (1995).
64. A. R. Bishop and R. G. Nuzzo, *Curr. Opin. Coll. Interf. Sci.*, **1**, 127 (1996).
65. G. E. Poirier, *Chem. Rev.*, **97**, 1117 (1997).
66. C. A. Widrig, C. A. Alves and M. D. Porter, *J. Am. Chem. Soc.*, **113**, 2805 (1991).
67. P. Fenter, A. Eberhardt and P. Eisenberger, *Science*, **266**, 1216 (1994).
68. Y. Li, J. Huang, R. T. McIver Jr. and J. C. Hemminger, *J. Am. Chem. Soc.*, **114**, 2428 (1992).
69. T. D. McCarley and R. L. McCarley, *Anal. Chem.*, **69**, 130 (1997).
70. C. D. Bain and G. M. Whitesides, *J. Am. Chem. Soc.*, **111**, 7164 (1989).
71. D. A. Buttry and M. D. Ward, *Chem. Rev.*, **92**, 1355 (1992).
72. D. S. Karpovich and G. J. Blanchard, *Langmuir*, **10**, 3315 (1994).
73. G. E. Poirier and E. D. Pylant, *Science*, **272**, 1145 (1996).

74. N. B. Larsen, H. A. Biebuyck, E. Delamarche and B. Michel, *J. Am. Chem. Soc.*, **119**, 3017 (1997).
75. N. Camillone III, C. E. D. Chidsey, P. Eisenberger, P. Fenter, J. Li, K. S. Liang, G.-Y. Liu and G. Scoles, *J. Chem. Phys.*, **99**, 744 (1993).
76. G.-Y. Liu, P. Fenter, C. E. D. Chidsey, D. F. Ogletree, P. Eisenberger and M. Salmeron, *J. Chem. Phys.*, **101**, 4301 (1994).
77. Y. Xia, X.-M. Zhao and G. M. Whitesides, *Microelectron. Eng.*, **32**, 255 (1996).
78. X.-M. Zhao, J. L. Wilbur and G. M. Whitesides, *Langmuir*, **12**, 3257 (1996).
79. C. Schonenberger, J. A. M. Sondag-Huethorst, J. Jorritsma and L. G. J. Fokkink, *Langmuir*, **10**, 611 (1994).
80. C. A. McDermott, M. T. McDermott, J.-B. Green and M. D. Porter, *J. Phys. Chem.*, **99**, 13257 (1995).
81. E. Delamarche, B. Michel, H. Kang and C. Gerber, *Langmuir*, **10**, 4103 (1994).
82. K. L. Prime and G. M. Whitesides, *J. Am. Chem. Soc.*, **115**, 10714 (1993).
83. D. J. Olbris, A. Ulman and Y. Shnidman, *J. Chem. Phys.*, **102**, 6865 (1995).
84. H. Schönherr and H. Ringsdorf, *Langmuir*, **12**, 3891 (1996).
85. T. Ishida, S. Yamamoto, W. Mizutani, M. Motomatsu, H. Tokumoto, H. Hokari, H. Azehara and M. Fujihara, *Langmuir*, **13**, 3261 (1997).
86. R. M. Overney, E. Meyer, J. Frommer, D. Brodbeck, R. Lüthi, H.-J. Güntherodt, L. Howald, M. Fujihara, H. Takano and Y. Gotoh, *Nature*, **359**, 133 (1992).
87. H. A. Biebuyck, C. D. Bain and G. M. Whitesides, *Langmuir*, **10**, 1825 (1994).
88. T. Takami, E. Delamarche, B. Michel, C. Gerber, H. Wolf, and H. Ringsdorf, *Langmuir*, **11**, 3876 (1995).
89. J. J. Hickman, D. Ofer, P. E. Laibinis, G. M. Whitesides and M. S. Wrighton, *Science*, **252**, 688 (1991).
90. S. J. Vigmond, M. Iwakura, F. Mizutani and T. Katsura, *Langmuir*, **10**, 2860 (1994).
91. J. M. Tour, L. Jones II, D. L. Pearson, J. J. S. Lamba, T. P. Burgin, G. M. Whitesides, D. L. Allara, A. N. Parikh and S. V. Atre, *J. Am. Chem. Soc.*, **117**, 9529 (1995).
92. P. E. Laibinis and G. M. Whitesides, *J. Am. Chem. Soc.*, **114**, 9022 (1992).
93. J. F. Dorsten, J. E. Maslar and P. W. Bohn, *Appl. Phys. Lett.*, **66**, 1755 (1995).
94. A. Kumar, H. A Biebuyck and G. M. Whitesides, *Langmuir*, **10**, 1498 (1994).
95. Y. Xia and G. M. Whitesides, *Angew. Chem. Int. Ed. Engl.*, **37**, 551 (1998).
96. Y. Xia, D. Qin and G. M. Whitesides, *Adv. Mater.*, **8**, 1015 (1996).
97. H. A. Biebuyck, N. B. Larsen, E. Delamarche and B. Michel, *IBM J. Res. Dev.*, **41**, 159 (1997).
98. A. Kumar and G. M. Whitesides, *Science*, **263**, 60 (1994).
99. H. A. Biebuyck and G. M. Whitesides, *Langmuir*, **10**, 2790 (1994).
100. R. Singhvi, A. Kumar, G. P. Lopez, G. N. Stephanopoulos, D. I. C. Wang, G. M. Whitesides and D. E. Ingber, *Science*, **264**, 696 (1994).
101. M. Mrksich, C. S. Chen, Y. Xia, L. E. Dike, D. E. Ingber and G. M. Whitesides, *Proc. Natl. Acad. Sci. USA*, **93**, 10775 (1996).
102. Y. Xia, E. Kim and G. M. Whitesides, *J. Electrochem. Soc.*, **143**, 1070 (1996).
103. A. Ulman, *Mater. Res. Soc. Bull.*, **20**, 46 (1995).
104. M. Mrksich and G. M. Whitesides, *TIBTECH*, **13**, 228 (1995).
105. M. Mrksich and G. M. Whitesides, *Annu. Rev. Biophys. Biomol. Struc.*, **25**, 55 (1996).
106. R. J. Jackman, J. L. Wilbur and G. M. Whitesides, *Science*, **269**, 664 (1995).
107. J. A. Zerkowski, C. T. Seto and G. M. Whitesides, *J. Am. Chem. Soc.*, **114**, 5473 (1992).
108. K. E. Schwiebert, D. N. Chin, J. C. MacDonald and G. M. Whitesides, *J. Am. Chem. Soc.*, **118**, 4018 (1996).
109. S. Palacin, D. N. Chin, E. E. Simanek, J. C. MacDonald, G. M. Whitesides, M. T. McBride and G. T. R. Palmore, *J. Am. Chem. Soc.*, **119**, 11807 (1997).

110. S. Y. Chou, P. R. Krauss and P. Renstron, *J. Appl. Phys. Lett.*, **67**, 3114 (1995).
111. M. C. Wu, L. Y. Lin and S. S. Lee, *SPIE*, **2291**, 40.
112. E. Smela, O. Inganäs and I. Lundström, *Science*, **268**, 1735 (1995).
113. J. H. E. Promislow and A. P. Gast, *Langmuir*, **12**, 4095 (1996).
114. A. W. Simpson and P. H. Hodkinson, *Nature*, **237**, 320 (1972).
115. S. T. Schober, J. Friedrich and A. Altmann, *J. Appl. Phys.*, **71**, 2206 (1992).
116. C. A. Mirkin, R. L. Letsinger, R. C. Mucic and J. J. Storhoff, *Nature*, **382**, 607 (1996).
117. J. Tien, A. Terfort and G. M. Whitesides, *Langmuir*, **13**, 5349 (1997).
118. M. A. Fortes, *Can. J. Chem.*, **60**, 2889 (1982).
119. P. A. Kralchevsky, V. N. Paunov, N. D. Denkov, I. B. Ivanov and K. Nagayama, *J. Coll. Interf. Sci.*, **155**, 420 (1993).
120. P. A. Kralchevsky and K. Nagayama, *Langmuir*, **10**, 23 (1994).
121. D. W. Fakes, M. C. Davies, A. Browns and J. M. Newton, *Surf. Interf. Anal.*, **13**, 233 (1988).
122. M. Yamaki, J. Higo and K. Nagayama, *Langmuir*, **11**, 2975 (1995).
123. N. D. Denkov, O. D. Velev, P. A. Kralchevsky, I. B. Ivanov, H. Yoshimura and K. Nagayama, *Langmuir*, **8**, 3183 (1992).
124. K. B. Lipkowitz and D. B. Boyd, *Rev. Comp. Chem.*, VCH: New York, 1990.
125. K. B. Lipkowitz and D. B. Boyd, *Rev. Comp. Chem.*, VCH: New York, 1991.
126. B. R. Brooks, R. E. Bruccoleri, B. D. Olafson, D. J. States, S. Swaminathan and M. L. Karplus, *J. Comp. Chem.*, **4**, 187 (1983).
127. M. P. Allen and D. J. Tildesley, *Computer Simulations of Liquids*, Clarendon Press, Oxford, 1987.
128. J. D. Turner, P. K. Weiner, H. Chun, V. Lupi, S. Gallion and U. C. Singh, in *Computer Simulation of Biomolecular Systems: Theoretical and Experimental Applications* (eds Gunsteren, W. F., Weiner, P. K. and Wilkinson, A. J.) EXCOM, Leiden, 1993.
129. A. M. Mathiowetz, A. Jain, N. Karasawa and W. A. Goddard, *Proteins*, **20**, 227 (1994).
130. T. Schlick and W. K. Olson, *Science*, **257**, 1110 (1992).
131. S. A. Allison, S. H. Northrup and J. A. McCammon, *Biophys. J.*, **49**, 167 (1986).
132. B. A. Luty, M. E. Davis and J. A. McCammon, *J. Comp. Chem.*, **13**, 768 (1992).
133. A. Nicholls and B. Honig, *J. Comp. Chem.*, **12**, 435 (1991).
134. D. L. Beveridge and F. M. Dicapua, *Annu. Rev. Biophys. Biophys. Chem.*, **18**, 431 (1989).
135. J. I. Siepmann and I. R. McDonald, *Mol. Phys.*, **75**, 255 (1992).
136. D. N. Chin, G. T. R. Palmore and G. M. Whitesides, *J. Am. Chem. Soc.* In press.
137. J. Perlstein, *J. Am. Chem. Soc.*, **114**, 1955 (1992).
138. J. Perlstein, *J. Am. Chem. Soc.*, **116**, 455 (1994).
139. H. R. Karfunkel and R. J. Gdanitz, *J. Comp. Chem.*, **13**, 1171 (1992).
140. A. Gavezzotti, *Acc. Chem. Res.*, **27**, 309 (1994).
141. A. Gavezzotti and G. Filippini, *J. Phys. Chem.*, **98**, 4831 (1994).
142. A. Gavezzotti, *J. Am. Chem. Soc.*, **113**, 4622 (1991).
143. A. Gavezzotti, *J. Phys. Chem.*, **94**, 4319 (1990).
144. M. C. Etter, *J. Phys. Chem.*, **95**, 4601 (1991).
145. J. A. Zerkowski, C. T. Seto, D. A. Wierda and G. M. Whitesides, *J. Am. Chem. Soc.*, **112**, 9025 (1990).
146. J. A. Zerkowski, J. C. MacDonald, C. T. Seto, D. A. Wierda and G. M. Whitesides, *J. Am. Chem. Soc.*, **116**, 2382 (1994).
147. J. A. Zerkowski and G. M. Whitesides, *J. Am. Chem. Soc.*, **116**, 4298 (1994).
148. J. A. Zerkowski, J. P. Mathias and G. M. Whitesides, *J. Am. Chem. Soc.*, **116**, 4305 (1994).
149. C. D. Dushkin, P. A. Kralchevsky, V. N. Paunov, H. Yoshimura and K. Nagayama, *Langmuir*, **12**, 641 (1996).

150. E. B. Throughton, C. D. Bain, G. M. Whitesides, R. G. Nuzzo, D. L. Allara and M. D. Porter, *Langmuir*, **4**, 365 (1988).
151. J. E. Chadwick, D. C. Myles and R. L. Garrell, *J. Am. Chem. Soc.*, **115**, 10364 (1993).
152. K. Uvdal, I. Persson and B. Liedberg, *Langmuir*, **11**, 1252 (1995).
153. P. Fenter, P. Eisenberger, J. Li, N. Camillone III, S. Bernasek, G. Scoles, T. A. Ramnanarayanan and K. S. Liang, *Langmuir*, **7**, 2013 (1991).
154. J. B. Schlenoff, M. Li and H. Ly, *J. Am. Chem. Soc.*, **117**, 12528 (1995).
155. T. R. Lee, P. E. Laibinis, J. P. Folkers and G. M. Whitesides, *Pure Appl. Chem.*, **63**, 821 (1991).
156. J. J. Hickman, P. E. Laibinis, D. I. Auerbach, C. Zou, T. J. Gardner, G. M. Whitesides and M. S. Wrighton, *Langmuir*, **8**, 357 (1992).
157. C. W. Sheen, J.-X. Shi, J. Martensson, A. N. Parikh and D. L. Allara, *J. Am. Chem. Soc.*, **114**, 1514 (1992).
158. Y. Gu, Z. Lin, R. A. Butera, V. S. Smentkowski and D. H. Waldeck, *Langmuir*, **11**, 1849 (1995).
159. M. J. Wirth, R. W. P. Fairbank and H. O. Fatunmbi, *Science*, **275**, 44 (1997).
160. M. R. Linford and C. E. D. Chidsey, *J. Am. Chem. Soc.*, **115**, 12631 (1993).
161. M. R. Linford, P. Fenter, P. M. Eisenberger and C. E. D. Chidsey, *J. Am. Chem. Soc.*, **117**, 3145 (1995).
162. A. Bansal, X. Li, I. Lauermann, N. S. Lewis, S. I. Yi and W. H. Weinberg, *J. Am. Chem. Soc.*, **118**, 7225 (1996).
163. Y.-T. Tao, M.-T. Lee and S.-C. Chang, *J. Am. Chem. Soc.*, **115**, 9547 (1993).
164. J. P. Folkers, C. B. Gorman, P. E. Laibinis, S. Buchholz, G. M. Whitesides and R. G. Nuzzo, *Langmuir*, **11**, 813 (1995).
165. G. Cao, H.-G. Hong and T. E. Mallouk, *Acc. Chem. Res.*, **25**, 420 (1992).
166. T. J. Gardner, C. D. Frisbie and M. S. Wrighton, *J. Am. Chem. Soc.*, **117**, 6927 (1995).
167. M. R. Anderson, M. N. Evaniak and M. Zhang, *Langmuir*, **12**, 2327 (1996).
168. N. Camillone III, T. Y. B. Leung, P. Schwartz, P. Eisenberger and G. Scoles, *Langmuir*, **12**, 2737 (1996).
169. W. B. Caldwell, D. J. Campbell, K. Chen, B. R. Herr, C. A. Mirkin, A. Malik, M. K. Durbin, P. Dutta and K. G. Huang, *J. Am. Chem. Soc.*, **117**, 6071 (1995).
170. L. Strong and G. M. Whitesides, *Langmuir*, **4**, 546 (1988).
171. M. A. Bryant and J. E. Pemberton, *J. Am. Chem. Soc.*, **113**, 3629 (1991).
172. Q. Du, E. Freysz and Y. R. Shen, *Science*, **264**, 826 (1994).
173. C. D. Bain, *J. Chem. Soc. Faraday Trans.*, **91**, 1281 (1995).
174. J. P. Folkers, P. E. Laibinis and G. M. Whitesides, *Langmuir*, **8**, 1330 (1992).
175. L. H. Dubois, B. R. Zegarski and R. G. Nuzzo, *J. Am. Chem. Soc.*, **112**, 570 (1990).
176. M. J. Tarlov and J. G. Newman, *Langmuir*, **8**, 1298 (1992).
177. C. D. Bain and G. M. Whitesides, *J. Am. Chem. Soc.*, **110**, 3665 (1988).
178. C. D. Bain, E. B. Throughton, Y.-T. Tao, J. Evall, G. M. Whitesides and R. G. Nuzzo, *J. Am. Chem. Soc.*, **111**, 321 (1989).
179. M. D. Ward and D. A. Buttry, *Science*, **249**, 1000 (1990).
180. S. Li and R. M. Crooks, *Langmuir*, **9**, 1951 (1993).
181. A. Badia, R. Back and R. B. Lennox, *Angew. Chem. Int. Ed. Engl.*, **33**, 2332 (1994).
182. Y. Xia, E. Kim, M. Mrksich and G. M. Whitesides, *Chem. Mater.*, **8**, 601 (1996).
183. J. Huang and J. C. Hemminger, *J. Am. Chem. Soc.*, **115**, 3342 (1993).
184. M. J. Tarlov, D. R. F. Burgess Jr. and G. Gillen, *J. Am. Chem. Soc.*, **115**, 5305 (1993).
185. K. C. Chan, T. Kim, J. K. Schoer and R. M. Crooks, *J. Am. Chem. Soc.*, **117**, 5875 (1995).
186. T. Kim, K. C. Chan and R. M. Crooks, *J. Am. Chem. Soc.*, **119**, 189 (1997).
187. E. W. Wollman, C. D. Frisbie and M. S. Wrighton, *Langmuir*, **9**, 1517 (1993).
188. D. J. Pritchard, H. Morgan and J. M. Cooper, *Angew. Chem. Int. Ed. Engl.*, **34**, 91 (1995).

189. J. A. M. Sondag-Huethorst, H. R. J. van Helleputte and L. G. Fokkink, *Appl. Phys. Lett.*, 64, 285 (1994).
190. M. Lercel, R. C. Tiberio, P. F. Chapman, H. G. Craighead, C. W. Sheen, A. N. Parikh and D. L. Allara, *J. Vac. Sci. Technol. B*, 11, 2823 (1993).
191. G. Gillen, S. Wight, J. Bennett and M. Tarlov, *J. Appl. Phys. Lett.*, 65, 534 (1994).
192. K. K. Berggren, A. Bard, J. L. Wilbur, J. D. Gillaspy, A. G. Helg, J. J. McClelland, S. L. Rolston, W. D. Phillips, M. Prentiss and G. M. Whitesides, *Science*, 269, 1255 (1995).
193. C. B. Ross, L. Sun and R. M. Crooks, *Langmuir*, 9, 632 (1993).
194. N. L. Abbott, A. Kumar and G. M. Whitesides, *Chem. Mater.*, 6, 596 (1994).
195. A. Kumar, H. A. Biebuyck, N. L. Abbott and G. M. Whitesides, *J. Am. Chem. Soc.*, 114, 9188 (1992).